Brn-1 and Brn-2 share crucial roles in the production and positioning of mouse neocortical neurons

Yoshinobu Sugitani,[1] Shigeyasu Nakai,[1] Osamu Minowa,[1,2] Miyuki Nishi,[1] Kou-ichi Jishage,[1] Hitoshi Kawano,[3] Kensaku Mori,[4] Masaharu Ogawa,[5] and Tetsuo Noda[1,2,6,7,8]

[1]Department of Cell Biology, JFCR–Cancer Institute, Tokyo 170-8455, Japan; [2]Mouse Functional Genomics Research Group, RIKEN Genomic Sciences Center, Kanagawa 244-0804, Japan; [3]Department of Developmental Morphology, Tokyo Metropolitan Institute for Neuroscience, Tokyo 183-8526, Japan; [4]Department of Physiology, Graduate School of Medicine, University of Tokyo, Tokyo 113-0033, Japan; [5]Laboratory for Cell Culture Development, Brain Science Institute, RIKEN, Saitama 351-0198, Japan; [6]Department of Molecular Genetics, Tohoku University School of Medicine, Miyagi 980-8575, Japan; [7]Core Research for Evolutional Science and Technology, Japan Science and Technology Corporation, Saitama 332-0012, Japan

Formation of highly organized neocortical structure depends on the production and correct placement of the appropriate number and types of neurons. POU homeodomain proteins Brn-1 and Brn-2 are coexpressed in the developing neocortex, both in the late precursor cells and in the migrating neurons. Here we show that double disruption of both *Brn-1* and *Brn-2* genes in mice leads to abnormal formation of the neocortex with dramatically reduced production of layer IV–II neurons and defective migration of neurons unable to express *mDab1*. These data indicate that Brn-1 and Brn-2 share roles in the production and positioning of neocortical neuron development.

Received January 22, 2002; revised version accepted May 23, 2002.

The mature neocortex is organized into six cell layers, each of which contains neurons with similar morphologies, molecular properties, and projection patterns. The development of this neocortical structure depends on a highly ordered pattern of neuronal production and migration. Cortical neurons that comprise each layer are sequentially produced in the ventricular zone of the dorsal telencephalon (Angevine and Sidman 1961; Takahashi et al. 1999). Although the regulatory factors that function in this sequential production of a variety of layer-specific neurons have not been identified in mammals, in *Drosophila* the successive production of different types of cells from neuroblasts has been found to require a temporally stereotyped pattern of expression of a set of transcription factors including the *Drosophila* POU transcription factors Pdm1 and Pdm2 (Isshiki et al. 2001). In mammals, newly produced neurons leave their birthplace, migrate toward the cortical surface, and form cortical layers in an inside-out pattern with respect to their time of birth (Angevine and Sidman 1961; Rakic 1972). Recent genetic studies have identified large numbers of functional molecules involved in the migration/positioning of neocortical neurons (for review, see Rice and Curran 1999).

Brn-1 and Brn-2, members of the mammalian class III POU transcription factor family, are prominently expressed in the embryonic brain, including the neocortex (He et al. 1989). Each single mutant, however, shows abnormalities only in limited brain regions. In *Brn-2* mutant neonates, neuronal loss was observed only in the hypothalamic supraoptic and paraventricular nuclei, where *Brn-1* is not expressed (Nakai et al. 1995; Schonemann et al. 1995). In *Brn-1* mutants, remarkable changes in brain morphology were observed only in the hippocampus, where Brn-2 expression is barely detectable (data not shown). In the neocortex, where both Brn-1 and Brn-2 are expressed, no overt developmental defects were seen in either single mutant. These observations suggest functional complementation between Brn-1 and Brn-2 in neocortical development.

Results and Discussion

To explore their possible overlapping functions in neocortical development, we generated *Brn-1/Brn-2* double homozygous mutants by intercrossing double heterozygotes that were healthy and fertile, with no apparent phenotype. Double homozygous mutants were born at the expected Mendelian ratio (76 double homozygous mutants among 1192 pups), but all of them died within 1 h after birth. In contrast to the limited abnormalities in *Brn-1*$^{-/-}$ or *Brn-2*$^{-/-}$ single mutants, *Brn-1/Brn-2* double mutants suffered severe, broad brain defects. The olfactory bulb showed hypoplasia (Fig. 1A,B), and the cerebellum was less foliated, with loosely packed Purkinje cells (Fig. 1C,D). The neocortex was severely affected; its thickness was markedly reduced, and the stratification of the cortical neurons appeared to be disorganized (Fig. 1E,F).

The hypoplastic neocortex could be caused by reduced cell proliferation or accelerated cell death during embryonic corticogenesis. Because there was no evidence of increased apoptosis in *Brn-1/Brn-2* double mutant cortex from embryonic day 14.5 (E14.5) to postnatal day 0 (P0; data not shown), we examined the proliferation of cortical progenitor cells by bromodeoxyuridine (BrdU) labeling. In mice, most cortical plate neurons are produced in the ventricular zone (VZ) or in the subventricular zone (SVZ) from E12.5 to E16.5 (The Boulder Committee 1970; Takahashi et al. 1999). Up to E13.5, there was no significant difference in the number of BrdU-labeled cells in the VZ of the double mutant embryos, compared with wild-type (E12.5: 100.0% ± 1.8% of wild-type; E13.5: 100.8% ± 2.2% of wild-type; Fig. 2A,A′). Reduced

[*Key Words*: POU; Brn-1; Brn-2; mDab1; neocortex]
[8]Corresponding author.
E-MAIL tnoda@ims.u-tokyo.ac.jp; FAX 81-35-394-3893.
Article and publication are at http://www.genesdev.org/cgi/doi/10.1101/gad.978002.

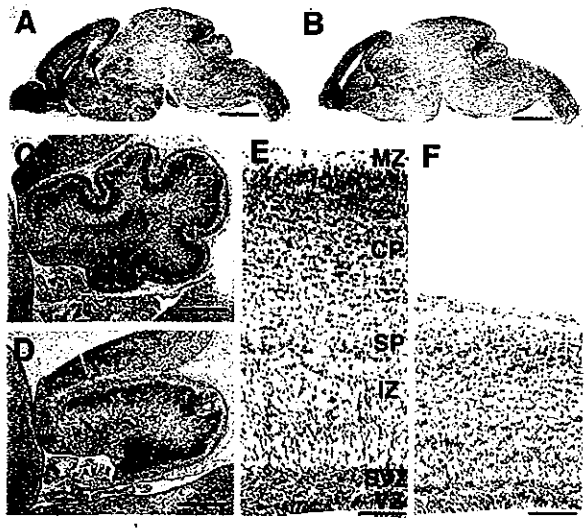

Figure 1. Morphological alterations in Brn-1/Brn-2 double mutant P0 brains. Sagittal sections of whole brain (HE stain) (*A,B*), cerebellum (brown, anti-Calbindin; blue, hematoxylin) (*C,D*), and neocortex (HE stain)(*E,F*) of wild-type (*A,C,E*) and Brn-1/Brn-2 double mutant (*B,D,F*) mice. Normally laminated structure consisting of the ventricular zone (VZ), subventricular zone (SVZ), intermediate zone (IZ), subplate (SP), cortical plate (CP), and marginal zone (MZ) is observed in wild-type neocortex (*E*), whereas, in Brn-1/Brn-2 mutant neocortex, the overall thickness is markedly reduced and the IZ is not clearly distinguishable from the CP (*F*). Scale bar: (*A,B*) 1 mm, (*C,D*) 200 μm, (*E,F*) 100 μm.

cell proliferation in the VZ was observed at E14.5 and thereafter in *Brn-1/Brn-2* mutant neocortex. (E14.5: 63.4% ± 2.6% of wild-type; E16.5: 60.2% ± 3.4% of wild-type; Fig. 2B,B′,C,C′). Reduction in the number of BrdU-labeled cells was particularly severe in the cortical SVZ in the double mutant (E16.5: 15.1% ± 2.5% of wild-type; Fig. 2C,C′). Despite the hypoplasticity of the Brn-1/Brn-2 deficient cortex, expression of GAD67 and calbindin appeared to be unaffected in the E19.0 neocortex (Fig. 3I,J; data not shown), suggesting intact generation and migration of the cortical interneurons, most of which are derived from the ganglionic eminence (Anderson et al. 1997). These results indicate that Brn-1 and Brn-2 share an essential role in the proliferation of cortical precursor cells within the VZ/SVZ from E14.5 onward, and that the reduction in subsequent cortical cell production could result in the hypoplastic neocortex seen in the double mutant neonate. Analysis of the temporal expression pattern for Brn-1 and Brn-2 proteins in the developing wild-type neocortex revealed that their expression in the VZ is initiated at ~E14.5 and is prominent thereafter in the VZ/SVZ (Fig. 2D–I), with a pattern that corresponds with the period of reduced cell proliferation in the neocortex of double mutant embryos. These results suggest that Brn-1 and Brn-2 may function in the proliferation of late cortical progenitor cells in a cell-autonomous manner.

Lineage analyses and birthdating studies suggest that common cortical precursor cells first produce neurons of layer VI and then layer V (at E11.5–E15.5) and, even later, generate neurons destined for layers IV–II (at E14.5–E17.0) by successive cell division (Luskin et al. 1988; Takahashi et al. 1999). From the late embryonic neurogenesis stage, glial progenitor cells also proliferate and increase their numbers (Berman et al. 1997), differentiating into astrocytes or oligodendrocytes during a postnatal stage. The finding that Brn-1 and Brn-2 function in cell proliferation, specifically at the late neurogenesis stage, prompted us to examine whether Brn-1 and Brn-2 function in the production of upper-layer neurons and/or in the generation/expansion of glial progenitor cells. We assessed the formation of each cortical layer and the status of gliogenesis in the double mutant cortex at E19.0 or E18.5, using the following markers for different layers and glial progenitors: *Tbr-1* for layer VI, subplate and SVZ (Fig. 3A); *Wnt7b* for layer VI (data not shown; Rubenstein et al. 1999), *ER81* for layer V (Fig. 3C); *RORβ* for layer IV (Fig. 3E; Weimann et al. 1999), *mSorLA* or *Svet1* for layers II/III and SVZ cells (Fig. 3G; data not shown; Hermans-Borgmeyer et al. 1998; Tarabykin et al. 2001),

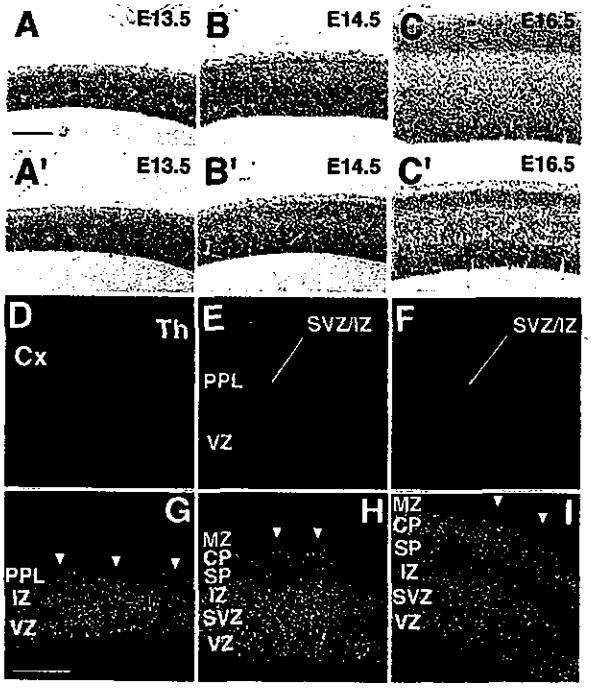

Figure 2. Reduced cell proliferation in Brn-1/Brn-2 mutant neocortex and expression of Brn-1 and Brn-2 in developing neocortex. BrdU labeling (brown) in sagittal sections of wild (*A–C*) and *Brn-1/Brn-2* mutant (*A′–C′*) neocortex at indicated stages. Fluorescent micrographs of sagittal sections of E12.5 (*D*), E13.5 (*E,F*), E14.5 (*G*), E15.5 (*H*), and E16.5 (*I*) cortices doubly stained with anti-Brn-1 (red) and anti-Brn-2 (green). Cells expressing both Brn-1 and Brn-2 appear yellow (*G–I*). All nuclei were stained with DAPI (blue) in *D–F*. Arrowheads indicate background staining by secondary antibodies in pia matter (*G–I*). From E13.5, Brn-1-expressing and Brn-2-expressing cells are clearly seen outside of the VZ in rostral and lateral cortex (*E,F*). From E14.5, Brn-1/Brn-2 coexpression also becomes prominent in the VZ/SVZ as well as in the IZ and the CP (*G–I*). Brn-1 or Brn-2 singularly expressing cells are also found within the MZ (*H,I*) or in the PPL (*G*) and the presumptive SP (*H,I*), respectively. (Cx) Neocortex, (Th) thalamus, (PPL) preplate. For other abbreviations, see Fig. 1. Scale bar: (*A–C,A′–C′*) 100 μm, (*D–I*) 200 μm.

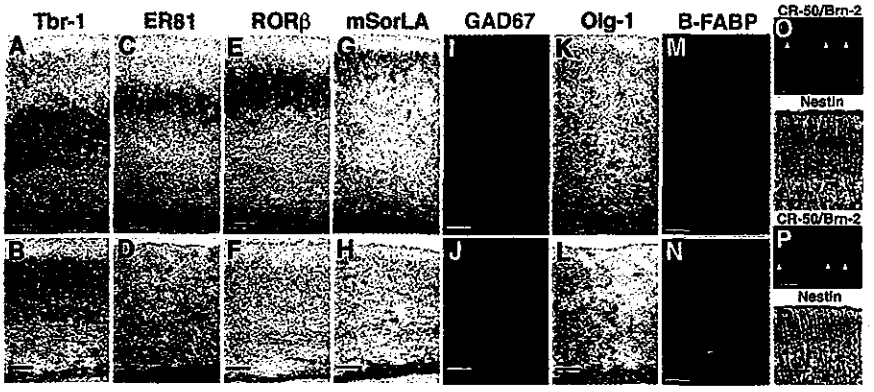

Figure 3. Loss of upper-layer neurons and altered positioning of cortical neurons in *Brn-1/Brn-2* mutant neocortex. In situ hybridization using *Tbr-1* (*A,B*), *ER81* (*C,D*), *RORβ* (*E,F*), *mSorLA* (*G,H*), *Olg-1* (*K,L*) riboprobes on coronal sections of E19.0 wild-type (*A,C,E,G,K*) and *Brn-1/Brn-2* mutant (*B,D,F,H,L*) cortices. In wild-type cortex, *Tbr-1*-positive layer VI, *ER81*-positive layer V, *RORβ*-positive layer IV, and *mSorLA*-positive layer II/III neurons are ordered from deep to superficial (*A,C,E,G*). In Brn-1/Brn-2 mutant cortex, however, the majority of the *ER81*-positive neurons are found beneath the *Tbr-1*-positive layer, with a few *ER81*-positive neurons detected in the superficial region within the cortical plate (*B,D*), and the numbers of layer IV or layer II/III neurons positive for *RORβ* or *mSorLA* are drastically reduced (*F,H*), although *mSorLA* expression is found in the SVZ with a similar pattern of *Tbr-1* expression in the SVZ (*H,B*). Immunostaining against GAD67 (red) (*I,J*), B-FABP (red) (*M,N*), Reelin (green) and Brn-2 (red) (*O,P*), and Nestin (brown) (*Q,R*) on sagittal (*M,N,Q,R*) and coronal (*I,J,O,P*) sections of E19.0 (*I,J*), E18.5 (*M–P*) and E16.5 (*Q,R*) cortices of wild-type (*I,M,O,Q*) and *Brn-1/Brn-2* mutant (*J,N,P,R*). Scale bar: (*A–N*) 100 μm, (*O,P*) 20 μm, (*Q,R*) 50 μm.

Olg-1 for oligodendrocyte progenitors (Fig. 3K; Lu et al. 2000; Zhou et al. 2000), B-FABP/BLBP for immature astrocytes and radial glial cells (Fig. 3M; Feng et al. 1994; Kurtz et al. 1994), and CR-50 for Cajal-Retzius neurons in the marginal zone (MZ; Fig. 3O; Ogawa et al. 1995; D'Arcangelo et al. 1997). The marker studies indicated that the initial step of gliogenesis seemed to be unaffected in *Brn-1/Brn-2* mutant neocortex (Fig. 3L,N), whereas the numbers of *RORβ*-positive, *mSorLA*-positive, or *Svet1*-positive neurons were dramatically reduced in *Brn-1/Brn-2* mutant neocortex with *mSorLA*-expressing or *Svet1*-expressing SVZ cells lining the entire surface of the enlarged lateral ventricles of the mutant brains (Fig. 3F,H; data not shown). These results suggest that Brn-1 and Brn-2 are essential for proper production of neocortical neurons destined for layers VI–II.

Molecular marker analysis also revealed abnormal layering of the remaining cortical neurons in Brn-1/Brn-2-deficient neocortex, in which the majority of *ER81*-positive layer V neurons, normally laminated above the *Tbr-1*-positive or *Wnt7b*-positive layer VI (Fig. 3A,C; data not shown), were found beneath the *Tbr-1*-positive or *Wnt7b*-positive layer (Fig. 3B,D; data not shown). It has been well documented that the laminar structure of the neocortex is built by migration of successively produced neurons in an inside-to-outside fashion, such that neurons born earlier reside in deeper layers, and those born later occupy more superficial layers within the cortical plate (CP) between the MZ and the subplate (SP). Thus, the largely inverted packing pattern of layer V and VI neurons in *Brn-1/Brn-2* mutant cortex can be caused by either abnormal cell migration or cell fate defects such that the timing of layer VI and layer V neuronogenesis is inverted. To distinguish between the two possibilities, we labeled E12.5, E13.5, and E14.5 embryos, stages during which layer VI–V neuronogenesis is at a peak, with BrdU and examined the localization of BrdU-positive cortical neurons in E19.0 embryos. If the abnormal lamination is caused by cell fate defects, BrdU-labeled neurons should appear in comparable positions in the wild-type and *Brn-1/Brn-2* mutant cortices. Conversely, if neuronal migration is affected, neurons labeled at the same time should occupy different positions in wild-type and mutant mice. In E19.0 wild-type cortex, cells born on E12.5 occupied the SP and the deepest part of layer VI (Fig. 4A), and most of the cells at E13.5 predominantly occupied layer VI above the E12.5-born cohort (Fig. 4B). The relative positions of E13.5-born to E12.5-born neurons in the Brn-1/Brn-2-deficient cortex at E19.0 (Fig. 4D,E) were comparable with those in their wild-type littermates (Fig. 4A,B). The positioning of E14.5-born neurons, however, was significantly altered. E14.5-born cells in wild-type cortex occupied layers V and IV in a superficial region of the CP (Fig. 4C), whereas those in Brn-1/Brn-2-deficient cortex remained in the intermediate zone (IZ), beneath the cohort of E12.5-born cells (Fig. 4F). Together with the abnormal localization of the layer V neurons in the IZ of *Brn-1/Brn-2* mutant cortex (Fig. 3D), these BrdU neural birthdating experiments suggest abnormal migration of the layer V neurons born after E13.5 in *Brn-1/Brn-2* mutant cortex (Fig. 4K′,L,L′).

Correct neuronal migration requires both radial glial fibers as guiding scaffolds for migrating neurons (Rakic 1972) and Cajal-Retzius neurons that play a key role in neuronal lamination by producing the secreted Reelin protein (Ogawa et al. 1995; Rice and Curran 1999). The alignment and density of radial glial fibers, labeled with antibodies against B-FABP or Nestin, were not altered (Fig. 3N,R). Furthermore, neither the number of Cajal-Retzius neurons nor their immunolabeling intensity for Reelin was changed in the Brn-1/Brn-2-deficient cortex (Fig. 3P). In fact, Cajal-Retzius neurons in the wild-type cortex expressed neither Brn-1 nor Brn-2 at E16.5 and E18.5 cortex (Fig. 3O; data not shown). Thus, the migration defects in the Brn-1/Brn-2-deficient cortex do not seem to be a consequence of a disrupted radial glial fiber system or a loss of Reelin-expressing Cajal-Retzius neurons. Given Brn-1/Brn-2 coexpression in migrating neurons both in the IZ and CP (Fig. 2E–I), the altered migration of Brn-1/Brn-2-deficient cortical neurons can be a result of cell-autonomous defects.

To investigate the molecular mechanisms underlying the neuronal migration defects in *Brn-1/Brn-2* mutant cortex, an RT-PCR analysis was performed on various genes involved in neuronal migration (Rice and Curran 1999). mDab1, VLDLR/ApoER2, and α3-integrin have been shown to function in positioning cortical neurons by mediating Reelin signal transduction. CDK5, p35 (one of the CDK5 activator subunits), Lis1 (Pafah1b1), and

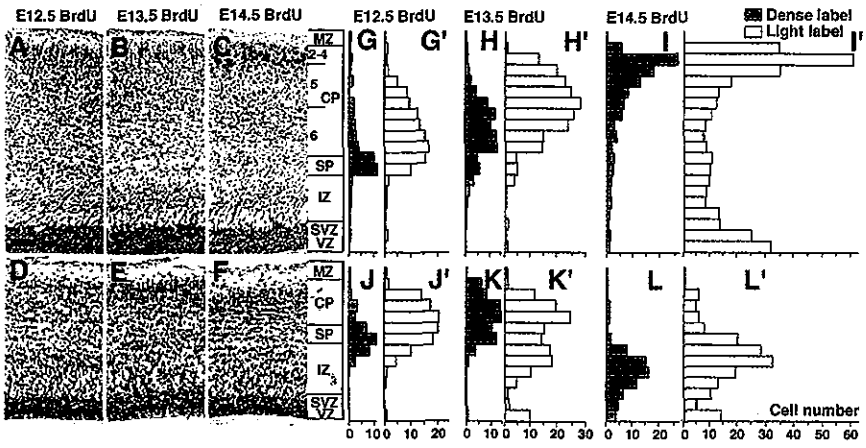

Figure 4. Abnormal migration of *Brn-1/Brn-2* mutant neurons. (*Left* panels) Distribution of cells labeled with BrdU during E12.5 (*A,D*), E13.5 (*B,E*), or E14.5 (*C,F*) in E19.0 wild-type (*A–C*) and *Brn-1/Brn-2* mutant (*D–F*) sagittal cortical sections. BrdU-positive nuclei (brown) were detected by immunohistochemistry. (*Right* panels) Bar graphs showing the radial distribution of heavily labeled cells (first generation at time of BrdU injection) (*G–L*) and lightly labeled cells (the majority of them are second and perhaps third generation cells from subsequent progenitor cell divisions) (*G′–L′*) in E19.0 wild-type (*G–I,G′–I′*) and *Brn-1/Brn-2* mutant (*J–L,J′–L′*) neocortex. In Brn-1/Brn-2 mutants, most E14.5 BrdU-labeled cells (*L,L′*) occupy the deepest positions. The subpopulation of E13.5 lightly labeled cells is also shifted to deeper positions (*K′*). (2–4) Layer II–VI, (5) Layer V, (6) Layer VI. For other abbreviations, see Fig. 1. Scale bar: 80 μm.

Doublecortin are also thought to affect neuronal migration in the developing cortex. Among all these tested genes, only *mdab1* expression was clearly affected in the *Brn-1/Brn-2* double mutant cortex at E16.5 (Fig. 5A,B; data not shown). Therefore, we examined the spatial distribution of the *mdab1* mRNA in the cortex of *Brn-1/Brn-2* mutant embryos and wild-type littermates by RNA in situ hybridization. In the wild-type cortex at E16.5, *mdab1* mRNA was expressed throughout the cortical wall, except for the MZ and SP. High levels of *mdab1* mRNA were detected in the upper regions of the IZ and in the CP (Fig. 5E; Rice and Curran 1999). In the Brn-1/Brn-2-deficient cortex at E16.5, *mdab1* mRNA expression was significantly reduced throughout the cortical wall and, in particular, was undetectable in the upper region of the IZ (Fig. 5F) just beneath the chondroitin sulfate proteoglycans (CSPG)-positive SP (Sheppard et al. 1991), in which p35-highly expressing late-born neurons were abnormally congested (Fig. 5H,J,L). Therefore, the slight reduction in *p35* mRNA levels in the E16.5 mutant cortex detected by RT-PCR analysis (Fig. 5A,B) might be caused by decreased numbers of *p35*-expressing neurons produced from E14.5 onward. Furthermore, quantitative RT-PCR analysis showed that *mdab1* expression was reduced also in *Brn-1/Brn-2* double heterozygotes (Fig. 5A,B), which show no histological defects in their neocortex. RNA in situ hybridization also showed that precipitously graded reduction of *mdab1* mRNA levels correlated well with Brn-1/Brn-2 gene dosages (data not shown). These results imply that Brn-1 and Brn-2 act genetically upstream to activate mDab1-dependent positioning processes in cortical neurons. The early-born neurons lacking Brn-1 and Brn-2, however, migrate and split the preplate into the MZ and SP properly (Fig. 5J), which is not seen in the *mdab1* mutant cortex; in *yotari* and *scrambler*, mutant mice carrying loss-of-function mutations in the *mdab1* gene, cortical neurons fail to split the preplate to form the CP between the MZ and SP (Rice and Curran 1999). The maintenance of integrity of preplate splitting in *Brn-1/Brn-2* mutant E16.5 cortex could be caused by the redundant function of another class III POU factor, Brn-4, that also shares high homology in its primary structure with Brn-1 and Brn-2 (Mathis et al. 1992). In wild-type as well as double-mutant cortex, *Brn-4* expression was also detected in the migrating neurons at ~E15.5, but was reduced after then (Fig. 5M–P). In Brn-1/Brn-2 mutant cortex, *mDab1* expression was detected until E15.5 (Fig. 5D) but was hardly detectable at E16.5 (Fig. 5F). Therefore, Brn-4, like Brn-1 and Brn-2, might also be able to activate mDab1-dependent processes in the positioning of early-born neurons.

Here we showed that there are two distinct types of the expression pattern of Brn-1/Brn-2 proteins in developing neocortex. Brn-1/Brn-2 expression in the precursor cells is restricted to a late pool of neural precursors, and Brn-1/Brn-2 is also expressed in a wide range of the postmitotic neurons, including *Tbr-1*-positive cortical plate neurons (data not shown). Double disruption of both *Brn-1* and *Brn-2* genes in mice led to two types of abnormalities during the neocortical development: selective loss of the neurons positive for layer IV–II markers (*RORβ*, *mSorLA*, and *Svet1*), and significantly reduced *mDab1* expression in all remaining neurons at late phase, independently of Brn-1/Brn-2 expression in their precursors.

Several lines of evidence suggest that mDab1 functions downstream of Reelin in a signaling pathway that controls cell positioning in the developing cortex (Rice and Curran 1999). However, it is not yet clear how these molecules dictate the spatial position of cortical neurons, including subplate neurons. Interestingly, in the Brn-1/Brn-2-deficient cortex, *mDab1* expression was severely reduced only at a late stage, when most of the E14.5-born neurons migrate through the IZ, but do not reach the MZ, remaining congested just beneath the SP. Therefore, these results imply that mDab1 may be necessary for CP neurons to migrate through the SP. Alternatively, Brn-1 and Brn-2 could also regulate expression of other molecules that may be essential in this process. On the other hand, the hypoplasticity of the Brn-1/Brn-2-deficient cortex cannot be explained by an inability to express *mdab1*, because reduced cell proliferation has not been reported in *mdab1* mutant cortex, and loss of *RORβ*-expressing or *mSorLA*-expressing neurons was not observed in *yotari* (data not shown). We examined *tailless* (Monaghan et al. 1997) and *pax6* (Tarabykin et al. 2001) expression, which are known to be essential for proper generation of cortical neurons. However, we found no changes in their expression in *Brn-1/Brn-2* mutant cortex (data not shown).

Previous reports have indicated that the earliest events

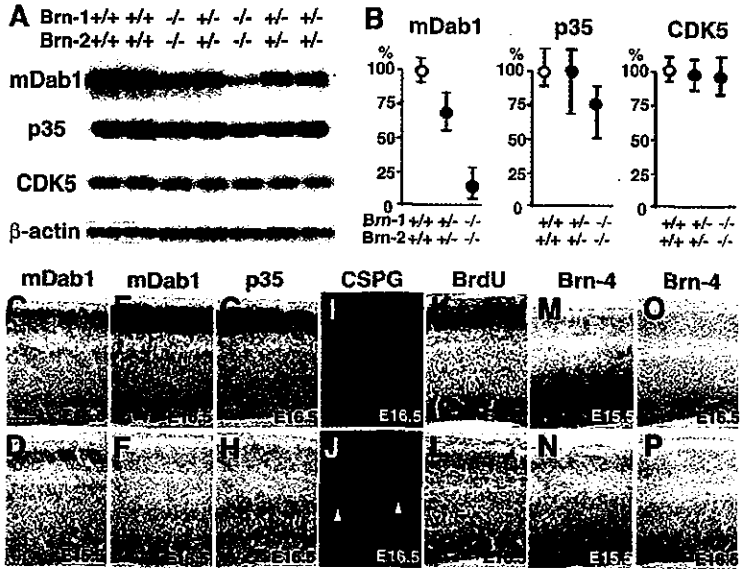

Figure 5. Reduced *mDab1* expression level and congestion of migrating neurons just beneath the subplate in Brn-1/Brn-2 mutant cortex. (*A*) RT-PCR analysis for *mDab1*, *p35*, *CDK5*, and β-*actin* mRNA expression in the E16.5 dorsal cortex of wild-type (+/+), Brn-1/Brn-2 double heterozygotes (+/−), and Brn-1/Brn-2 double homozygotes (−/−), and (*B*) quantitation of their mRNA levels in Brn-1/Brn-2 double heterozygotes ($n = 5$) and Brn-1/Brn-2 double homozygotes ($n = 5$) relative to those of wild-type embryos ($n = 4$). In situ hybridization using *mDab1* (*C–F*), *p35* (*G,H*), and *Brn-4* (*M–P*) riboprobes (blue) and immunostaining against CSPGs (green) (*I,J*) and BrdU labeled at E14.5 (brown) (*K,L*) on sagittal sections of E15.5 (*C,D,M,N*) and E16.5 (*E–L,O,P*) wild-type (*C,E,G,I,K,M,O*) and *Brn-1/Brn-2* mutant (*D,F, H,J,L,N,P*) cortices. All nuclei were stained with DAPI (blue) in *I* and *J*. Although *mDab1* expression is detected in wild-type and Brn-1/Brn-2 mutant cortices (*C,D*) at E15.5 when *Brn-4* is expressed (*M,N*), it is hardly detectable in E16.5 mutant cortex (*F*) when and where Brn-4 expression is decreased (*P*). The *p35*-expressing neurons in Brn-1/Brn-2 mutant cortex are less abundant in the CP and more so in the IZ beneath the SP (*H*) compared with wild-type (*G*). Immunolabeling for CSPGs, which is intense in the MZ and the SP (*I,J*), shows proper splitting of the preplate into the MZ and SP and abnormal cell congestion just beneath the CSPG-positive SP (white arrowheads) in Brn-1/Brn-2 mutant cortex (*J*). In the wild-type cortex, the majority of E14.5-born neurons are found in the IZ, and some of them have already entered into the CP (*K*), whereas in Brn-1/Brn-2 mutant cortex, none of the E14.5-born cells are found in the CP, and all of them stay beneath the presumptive SP (*L*). Scale bar: (*C–P*) 100 μm.

of cell class specification within each cortical layer occur in coordination with neuronogenesis within the proliferating zone (McConnell and Kaznowski 1991). At later stages, when superficial layers are being generated, the progenitors become restricted to an upper-layer fate (Frantz and McConnell 1996). A recent report suggests that the subpopulation of the SVZ cells derived from the VZ represents neuronal progenitors committed to upper-layer neurons (Tarabykin et al. 2001). Because Brn-1 and Brn-2 are specifically expressed in late precursor cells within the cortical VZ/SVZ and function in the proliferation of these cells both in the VZ and especially in the SVZ, these factors might share an intrinsic role in the production of fate-committed neuronal precursors and/or cortical neurons destined for the upper layers. Further analysis on these overlapping mutants would provide insight into the developmental mechanisms of the mammalian neocortex with its great diversity of cortical neurons.

Materials and methods

Histology and immunohistochemistry for calbindin, BrdU, and Nestin

Fixed samples in Bouin's fixative were dehydrated and embedded in paraffin blocks, from which 5–8-μm serial sections were cut. Hematoxylin and eosin (HE) staining was performed following standard protocols. For immunohistochemistry, the following antibodies were used: anti-Calbindin (a gift of M. Watanabe, Hokkaido University, Japan), anti-BrdU (Beckton Dickinson), anti-Nestin (a gift of Y. Tomooka, Science University of Tokyo, Japan), and anti-Pax6 (a gift of N. Osumi, Tohoku University, Japan). The Vectastain ABC kit (Vector Laboratories) was used for detection. The sections were counterstained with hematoxylin.

BrdU-labeling analysis

For the cell proliferation assay, we injected pregnant mice intraperitoneally with BrdU (50 mg/kg) 1.0 h before death. BrdU-positive cells were visualized as described above. Three embryos for each genotype were analyzed at the indicated stages, and 10 sagittal sections at the level of the olfactory bulb for each embryo were used. The fraction of BrdU-positive cells in the VZ was determined by dividing the number of BrdU-positive nuclei by the total number of the nuclei identified in units of the 200-μm-wide VZ. For the assay in the SVZ, because of the difficulty in distinguishing SVZ cells from postmitotic cells, BrdU-positive SVZ cells were counted in the same units as the assay in the VZ. For birthdating analysis to determine the distributions of the cells labeled with BrdU (30 mg/kg) in the E19.0 neocortical wall, parasagittal sections at the level of the accessory olfactory bulb were used. At the level, 500-μm-wide radial stripes in the medial portions were divided into ~40-μm-deep bins (20 horizontal bins in wild-type cortex and 14 bins in mutant cortex, respectively), and the position of each heavily and lightly labeled cell was assigned to a bin to generate histograms of the number of labeled cells against depth. Data from five sections from each of two to three littermates were averaged to give the histograms.

Immunofluorescence, apoptosis assay, and RNA in situ hybridization

Fixed samples with 4% paraformaldehyde in PBS were embedded in OCT compound, and serial sections (6–30 μm) were cut using a cryostat and immunostained with the following primary antibodies: anti-GAD (Chemicon, 1:1500 dilution), anti-B-FABP (a gift of F. Spener, University of Münster, Germany), CR-50 (1:100 dilution), anti-Brn-1 (Santa Cruz, 1:80 dilution), anti-CSPGs (Sigma, 1:600 dilution), and anti-Brn-2 (1:800 dilution). Anti-*Brn-2* rabbit polyclonal antibodies were raised against the C terminus of Brn-2 (amino acids 422–433). Western blot analysis and immunostaining confirmed the specificity of the antibodies. Apoptosis in the cortex at E14.5–P0 was assayed by using a TUNEL assay kit (Oncor). RNA in situ hybridization was performed by modified protocols as described earlier (Minowa et al. 1999). Riboprobes were synthesized using the following murine cDNAs: *mdab1* (30–464), *p35* (1142–1791), *Brn-4* (2219–2600), *Tbr-1* (2207–2956), *Wnt7b* (1138–1449), *mSorLA* (5320–6101), *Svet1* (2622–3243), and *tailless* (729–1410).

RT-PCR analysis

Total RNA (7.5 μg), extracted from dissected E16.5 dorsal cortices of each embryo, were reverse-transcribed with an oligo(dT) primer (Invitrogen), and 1/20 of each RT reaction was subjected to PCR amplification using specific primer pairs. The β-*actin* gene was used as control. The primer pairs used were mDab1, 5′-GGGCTGGAGAGCGCGTTTGAGTGCG-3′, 5′CTTCATCATGGAATCTTGACATAAC-3′; p35, 5′-TCGGCTGC TGACCACTCACTTTCCG-3′, 5′-AACAAAGATCACGGGCACCAGC GAG-3′; CDK5, 5′-CTAATGCAGGACGACCTCTCTTCCC-3′, 5′-TCA GCATCCCACACCCGACTCTTCC-3′; and β-actin (5′-CCTTCAACAC CCCAGCCATG-3′, 5′-TGCGCTCAGGAGGAGCAATG-3′. The PCR

products obtained were subjected to electrophoresis, and the intensities of each amplified band were analyzed by densitometry. The PCR products for mDab1, p35, CDK5, and β-actin were transferred to nylon-based membranes and hybridized with the following ^{32}P-labeled oligonucleotides specific for each cDNA: mDab1, 5′AAGGTCAGGATCGCAGC GAAGCCAC-3′; p35, 5′-TCCCCACTGTCCCATGATCGGAGCTG-3′; CDK5, 5′-CCCCATAGGCTCTCTGAACCCCAGT-3′; and β-actin, 5′-CAAGTCATCACTATTGGCAACGA-3′. For relative quantitation of *mDab1*, *p35*, and *CDK5* mRNA, the radioactivity of the amplified bands was quantitated relative to standard curves obtained by PCR amplification of serially diluted wild-type RT-products.

Acknowledgments

We thank M. Watanabe, Y. Tomooka, F. Spener, and N. Osumi for their gifts of rabbit polyclonal antibodies; and K. Okubo, T.M. Jessell, S.K. McConnell, and D.H. Rowritch for their gifts of the *doublecortin*, the *ER81*, the *RORβ*, and the *Olg-1* probes.

The publication costs of this article were defrayed in part by payment of page charges. This article must therefore be hereby marked "advertisement" in accordance with 18 USC section 1734 solely to indicate this fact.

References

Anderson, S.A., Eisenstat, D.D., Shi, L., and Rubenstein, J.L. 1997. Interneuron migration from basal forebrain to neocortex: Dependence on Dlx genes. *Science* **278:** 474–476.

Angevine, J.B. and Sidman, R.L. 1961. Autoradiographic study of cell migration during histogenesis of the cerebral cortex in the mouse. *Nature* **192:** 766–768.

Berman, N.E., Johnson, J.K., and Klein, R.M. 1997. Early generation of glia in the intermediate zone of the developing cerebral cortex. *Brain Res. Dev. Brain Res.* **101:** 149–164.

The Boulder Committee. 1970. Embryonic vertebrate central nervous system: Revised terminology. *Anat. Rec.* **166:** 257–261.

D'Arcangelo, G., Nakajima, K., Miyata, T., Ogawa, M., Mikoshiba, K., and Curran, T. 1997. Reelin is a secreted glycoprotein recognized by the CR-50 monoclonal antibody. *J. Neurosci.* **17:** 23–31.

Feng, L., Hatten, M.E., and Heintz, N. 1994. Brain lipid-binding protein (BLBP): A novel signaling system in the developing mammalian CNS. *Neuron* **12:** 895–908.

Frantz, G.D. and McConnell, S.K. 1996. Restriction of late cerebral cortical progenitors to an upper-layer fate. *Neuron* **17:** 55–61.

He X., Treacy, M.N., Simmons, D.M, Ingraham, H.A., Swanson, L.W., and Rosenfeld, M.G. 1989. Expression of a large family of POU-domain regulatory genes in mammalian brain development. *Nature* **340:** 35–41.

Hermans-Borgmeyer, I., Hampe, W., Schinke, B., Methner, A., Nykjaer, A., Susens, U., Fenger, U., Herbarth, B., and Schaller, H.C. 1998. Unique expression pattern of a novel mosaic receptor in the developing cerebral cortex. *Mech. Dev.* **70:** 65–76.

Isshiki, T., Pearson, B., Holbrook, S., and Doe, C.Q. 2001. *Drosophila* neuroblasts sequentially express transcription factors which specify the temporal identity of their neuronal progeny. *Cell* **106:** 511–521.

Kurtz, A., Zimmer, A., Schnutgen, F., Bruning, G., Spener, F., and Muller, T. 1994. The expression pattern of a novel gene encoding brain-fatty acid binding protein correlates with neuronal and glial cell development. *Development* **120:** 2637–2649.

Lu, Q.R., Yuk, D., Alberta, J.A., Zhu, Z., Pawlitzky, I., Chan, J., McMahon, A.P., Stiles, C.D., and Rowitch, D.H. 2000. Sonic hedgehog: Regulated oligodendrocyte lineage genes encoding bHLH proteins in the mammalian central nervous system. *Neuron* **25:** 317–329.

Luskin, M.B., Pearlman, A.L., and Sanes, J.R. 1988. Cell lineage in the cerebral cortex of the mouse studied in vivo and in vitro with a recombinant retrovirus. *Neuron* **8:** 635–647.

Mathis, J.M., Simmons, D.M., He, X., Swanson, L.W., and Rosenfeld, M.G. 1992. Brain 4: A novel mammalian POU domain transcription factor exhibiting restricted brain-specific expression. *EMBO J.* **11:** 2551–2561.

McConnell, S.K. and Kaznowski, C.E. 1991. Cell cycle dependence of laminar determination in developing neocortex. *Science* **254:** 282–285.

Minowa, O., Ikeda, K., Sugitani, Y., Oshima, T., Nakai, S., Katori, Y., Suzuki, M., Furukawa, M., Kawase, T., Zheng, Y., et al. 1999. Altered cochlear fibrocytes in a mouse model of DFN3 nonsyndromic deafness. *Science* **285:** 1408–1411.

Monaghan, A.P., Bock, D., Gass, P., Schwager, A., Wolfer, D.P., Lipp, H.P., and Schutz, G. 1997. Defective limbic system in mice lacking the tailless gene. *Nature* **390:** 515–517.

Nakai, S., Kawano, H., Yudate, T., Nishi, M., Kuno, J., Nagata, A., Jishage, K., Hamada, H., Fujii, H., Kawamura, K., et al. 1995. The POU domain transcription factor Brn-2 is required for the determination of specific neuronal lineages in the hypothalamus of the mouse. *Genes & Dev.* **9:** 3109–3121.

Ogawa, M., Miyata, T., Nakajima, K., Yagyu, K., Seike, M., Ikenaka, K., Yamamoto, H., and Mikoshiba, K. 1995. The reeler gene-associated antigen on Cajal-Retzius neurons is a crucial molecule for laminar organization of cortical neurons. *Neuron* **14:** 899–912.

Rakic, P. 1972. Mode of cell migration to the superficial layers of fetal monkey neocortex. *J. Comp. Neurol.* **145:** 61–83.

Rice, D.S. and Curran, T. 1999. Mutant mice with scrambled brains: Understanding the signaling pathways that control cell positioning in the CNS. *Genes & Dev.* **13:** 2758–2773.

Rubenstein, J.L., Anderson, S., Shi, L., Miyashita-Lin, E., Bulfone, A., and Hevner, R. 1999. Genetic control of cortical regionalization and connectivity. *Cereb. Cortex* **9:** 524–532.

Schonemann, M.D., Ryan, A.K., McEvilly, R.J., O'Connell, S.M., Arias, C.A., Kalla, K.A., Li, P., Sawchenko, P.E., and Rosenfeld, M.G. 1995. Development and survival of the endocrine hypothalamus and posterior pituitary gland requires the neuronal POU domain factor Brn-2. *Genes & Dev.* **9:** 3122–3135.

Sheppard, A.M., Hamilton, S.K., and Pearlman, A.L. 1991. Changes in the distribution of extracellular matrix components accompany early morphogenetic events of mammalian cortical development. *J. Neurosci.* **11:** 3928–3942.

Takahashi, T., Goto, T., Miyama, S., Nowakowski, R.S., and Caviness, V.S., Jr. 1999. Sequence of neuron origin and neocortical laminar fate: Relation to cell cycle of origin in the developing murine cerebral wall. *J. Neurosci.* **19:** 10357–10371.

Tarabykin, V., Stoykova, A., Usma, N., and Gruss, P. 2001. Cortical upper layer neurons derive from the subventricular zone as indicated by Svet1 gene expression. *Development* **128:** 1983–1993.

Weimann, J.M., Zhang, Y.A., Levin, M.E., Devine, W.P., Brulet, P., and McConnell, S.K. 1999. Cortical neurons require Otx1 for the refinement of exuberant axonal projections to subcortical targets. *Neuron* **24:** 819–831.

Zhou, Q., Wang, S., and Anderson, D.J. 2000. Identification of a novel family of oligodendrocyte lineage-specific basic helix–loop–helix transcription factors. *Neuron* **25:** 331–343.

RT-PCR analysis of *Tecta*, *Coch*, *Eya4* and *Strc* in mouse cochlear explants

Yukihide Maeda,[1,2] Kunihiro Fukushima,[2,CA] Masashi Kakiuchi,[2] Yorihisa Orita,[2] Kazunori Nishizaki[2] and Richard J. H. Smith[1]

[1]Molecular Otolaryngology Research Laboratory, Department of Otolaryngology, The University of Iowa Hospitals and Clinics, Iowa City, IA 52242, USA; [2]Department of Otolaryngology – Head and Neck Surgery, Okayama University Graduate School of Medicine, Okayama 700-8558, Japan

[CA]Corresponding Author: kuni@cc.okayama-u.ac.jp

Received 15 December 2004; accepted 17 December 2004

Tecta, *Coch*, *Eya4* and *Strc* are mouse orthologs of four human deafness-associated genes. Their expression is markedly restricted to specific cell types in cochleae. Cochleae were dissected on embryonic day 15 and cultured *in vitro*. Relative messenger RNA abundance of each gene was quantified by RT-PCR and compared in-vivo cochleae of equivalent embryonic age. After 48 h in culture, in-vivo and explant *Strc* expression levels were equivalent, *Eya4* level reduced in explanted tissues, and expression of *Tecta* and *Coch* did not show the expected temporal rise. Expression of these genes was detectable even after 96 h. These results suggest that it is feasible to test the expression of inner ear specific genes in explanted cochleae. *NeuroReport* 16:361–365 © 2005 Lippincott Williams & Wilkins.

Key words: Deafness-associated genes; Embryonic cochlea; Organ culture of cochlea; Quantitative RT-PCR

INTRODUCTION

The mammalian cochlea is unique in its architecture and variety of highly specialized cells that subserve the physiological process of sound transduction. This degree of cellular and function specificity is reflected by the number of genes that are expressed only or predominantly in the inner ear. Included in this list are *TECTA*, *COCH*, *EYA4* and *STRC*, allele variants of which cause nonsyndromic hearing loss at the DFNA8/12 [1], DFNA9 [2], DFNA10 [3] and DFNB16 [4] loci, respectively.

TECTA encodes α-tectorin, the major noncollagenous extracellular matrix protein of the tectorial membrane. *Tecta* messenger RNA is expressed in supporting cells of the mouse premature organ of Corti from embryonic day 12 (E12) and reaches its highest levels of expression on postnatal day 3 (P3). Thereafter, expression dramatically decreases although low levels persist from P45 to P67, with mean messenger RNA abundance after P15 being <25% of P3 levels [5–7].

COCH (coagulation factor C homolog) is also an extracellular matrix protein. It is expressed in fibrocytes of the spiral limbus and spiral ligament, and in fibrocytes of the connective tissue stroma underlying the sensory epithelium of the crista ampullaris of the semicircular canals. These sites correspond to the regions of the inner ear that show histological abnormalities in persons with DFNA9-related deafness [8,9]. Although it is the most abundant inner ear protein, its function is still unknown.

EYA4 encodes a transcriptional activator that is initially preferentially expressed in the ventral wall of the cochlear duct within cells that develop into the stria vascularis and Reissner's membrane. Expression peaks at E18.5, when *EYA4* is found preferentially in the dorsal half of the duct epithelium and in the greater and lesser epithelial ridges, especially in the basal turn. At older ages, expression becomes more restricted to cells derived from the spiral limbus, organ of Corti and spiral prominence [3].

STRC (stereocilin) is an integral protein of hair cells, where it is associated with the stereocilia. Expression in the murine cochlea appears first in the inner hair cells and then in the outer hair cells, probably reflecting earlier differentiation of stereocilia in the former. *STRC* is related in sequence to otoancorin and, on the basis of predicted GPI anchoring, may mediate attachment of the tectorial and otoconial membranes to sensory hair bundles [4].

During mouse development, the cochlear duct starts to differentiate from the otocyst at approximately E12. From the dorsal wall of its neuroepithelia, sensory hair cells and supporting cells differentiate between E13 and E18 [10], with ultrastructural maturation of hair cell stereocilia continuing until the second postnatal week [11]. The ventral wall of the immature cochlear duct and its lateral part are the anlage of Reissner's membrane and the epithelial wall of the stria vascularis that develop between E16 and P3 [10]. Components of the tectorial membrane are produced in the supporting cells in the premature organ of Corti between E15 and P5 [12]. The spiral limbus develops from the epithelial layer and underlying mesenchyme from E16 to P3 [10], and in the lateral wall of the cochlea, cells in the spiral ligament form the spiral prominence from E19 to P1 [11].

According to developmental stage and process of interest during morphogenesis, several types of in-vitro organ

culture of murine cochleae have been introduced. When fetal cochleae are dissected with the entire otocyst on E13 [13], either in their entirety at the level of the ductus reunions or with the vestibule and surrounding tissue on E15 [14,15], the premature cochlear duct and the neuroepithelia continue normal development *in vitro* for short time periods, typically under 6 days. Microdissection and culture of the neonatal organ of Corti also demonstrate that in-vitro morphology is comparable to that seen during normal development, including the innervation pattern to the organ of Corti [16] and the ultrastructure of the sensory hair cells [17].

These observations suggest that explanted cochleae should be valuable for investigating expressions of cochlear-specific genes. To test this hypothesis, we examined expression of *Tecta*, *Coch*, *Eya4* and *Strc* after explanting cochleae on E15 – a time when the cochlear duct has formed and the sensory and supporting cells have begun to differentiate. Relative messenger RNA abundance of these genes was determined by semiquantitative RT-PCR and compared with in-vivo cochleae of the corresponding embryonic age. As a control, we studied expression of *Gapdh*, a housekeeping gene encoding a glycolytic enzyme.

METHODS

Tissue dissection and culture of the mouse cochlea: Timed-pregnant female BALB/C mice were sacrificed using sodium pentobarbital (150 mg/kg, intraperitoneal) on E15 (vaginal plug, E0). The fetal cochleae were promptly dissected in ice-cold Dulbecco's modified Eagle's medium (DMEM) under a binocular microscope, identifying the cochlear duct at its basal and medial turns by removing the cochlear capsule. The isolated tissue contained the cochlear duct and immature sensory epithelium, nonneuronal mesenchymal tissues, lateral wall of cochlea and spiral neurons.

Explanted cochleae were placed in 500 µl of a serum-free medium that contained DMEM and Ham's F-12, supplemented with insulin (15 µg/ml), transferrin (20 µg/ml), progesterone (2×10^{-8} M), selenium (3×10^{-8} M) and putrescine (10^{-4} M). The medium was maintained at 37°C in 5% CO_2 and changed daily. Cochleae were maintained for 2 days (DIV2, for 48 h, n=6) and 4 days (DIV4, for 96 h, n=6) *in vitro* before extracting RNA. Control cochleae on E15 (n=5), E17 (n=7) and E19 (n=6) were dissected, immediately frozen in liquid nitrogen, and processed for RNA extraction. Usually, 8–12 cochleae from a single litter were processed in each sample. Formalin-fixed cryostat sections (10 µm) were obtained from cochleae on E15, DIV2 and DIV7. Sections were stained with 0.1% toluidine blue.

RNA extraction and reverse transcription: Total RNA was purified, treated with DNaseI (RNAse-Free DNAse set, Qiagen, Hilden, Germany), and quantified by measuring absorbancy at 260/280 nm as previously described [7]. Total RNA (3.5–7 µg) was typically purified from each in-vitro and in-vivo tissue sample. Total RNA (500 ng) was reverse transcribed in a 20 µl reaction; reverse transcriptase was omitted as a negative control.

PCR and data analysis: We followed a previously described protocol of semiquantitative RT-PCR with CCD imaging in which quantified band intensity is correlated linearly with the amount of RNA template [7,18]. Primer pairs for *Coch* (c.c.1346–1365 sense; c.c.1549–1568 antisense), *Eya4* (c.c.1705–1724; cc.1908–1927) and *Strc* (c.c.4934–4953; c.c.5166–5185) spanned the cDNA sequences in their conserved regions of the vWFA2 domain, *eya* homology region and C-terminal hydrophobic segments, respectively. The *Tecta* (c.c.6074–6093; cc.6254–6273) and *Gapdh* (c.c.650–669; cc.976–995) primers have been previously described. Each PCR (50 µl) was performed using 4 µl of the RT mixture [7].

After thermocycling in exponential phases, band intensity value (BIV) was determined by densitometry of the ethidium bromide luminescence of the PCR products on 3% agarose gels. After subtraction of background values as determined in an adjacent band-free area, BIVs from different gels were standardized to those of the same samples loaded on each gel. To assess expression of each gene, relative abundance (RA) of messenger RNA was expressed as the percentage of BIV to mean BIVs observed in E15 samples. Differences between groups were tested using one-way ANOVA and the post-hoc Bonferroni method. Significance was tested by confidence intervals of 99%, or as otherwise specified.

RESULTS

RT-PCR of *Tecta*, *Coch*, *Eya4*, *Strc* and *Gapdh* generated products of appropriate lengths; negative control RT-PCR resulted in no amplified product. Log[BIVs] of *Tecta*, *Coch*, *Eya4*, *Strc* and *Gapdh* linearly correlated with the number of amplification cycles in the exponential ranges of 22–30 (r=0.973, $p<0.01$), 21–29 (r=0.956, $p<0.01$), 23–31 (r=0.976, $p<0.01$), 23–31 (r=0.968, $p<0.01$) and 15–24 (r=0.972, $p<0.01$), respectively, using 100 ng of E15 RNA per PCR reaction. In addition, when 25, 50, 100, 200 or 400 ng of E15 RNA was used for each RT-PCR with *Tecta* primers, BIVs correlated with the amount of RNA added per PCR reaction ($p<0.05$). Therefore, BIVs of each sample were determined following 26 (*Tecta*), 25 (*Coch*), 28 (*Eya4*), 28 (*Strc*) and 20 (*Gapdh*) thermocycles, using 100 ng of total RNA per PCR reaction.

Figure 1a summarizes RT-PCR results as a percentage of the RA of *Tecta*, *Coch* , *Eya4*, *Strc* and *Gapdh* messenger RNA. Representative PCR bands obtained for each gene on E17 and DIV2 are shown in Fig. 1b.

The mean relative abundance (MRA) of *Tecta* increased between E15 (100±15%, RA, mean±SD) and E17 (157±55%) and remained at this level on E19 (161±37%), consistent with observations that *Tecta* expression increases between E15 and P3 by 50–60% [7]. In cochlear explants, in contrast, MRA of *Tecta* on DIV2 (25±12%) was significantly reduced compared with E15, and thus lower than E17 ($p<0.01$; Fig. 1b, row 1). MRA on DIV4 (11±11%) remained at a level equivalent to expression on DIV2 ($p>0.05$) and was significantly lower than on E19 ($p<0.01$).

MRA of *Coch* increased more than two-fold from E15 (100±26%) to E17 (246±62%) *in vivo* ($p<0.01$), and remained at this level on E19 (264±60%). In contrast, MRA on DIV2 (55±26%) decreased from E15 and was significantly lower than on E17 ($p<0.01$; Fig. 1b, row 2). MRA on DIV4 (60±27%) remained constant and was significantly lower than on E19 ($p<0.01$).

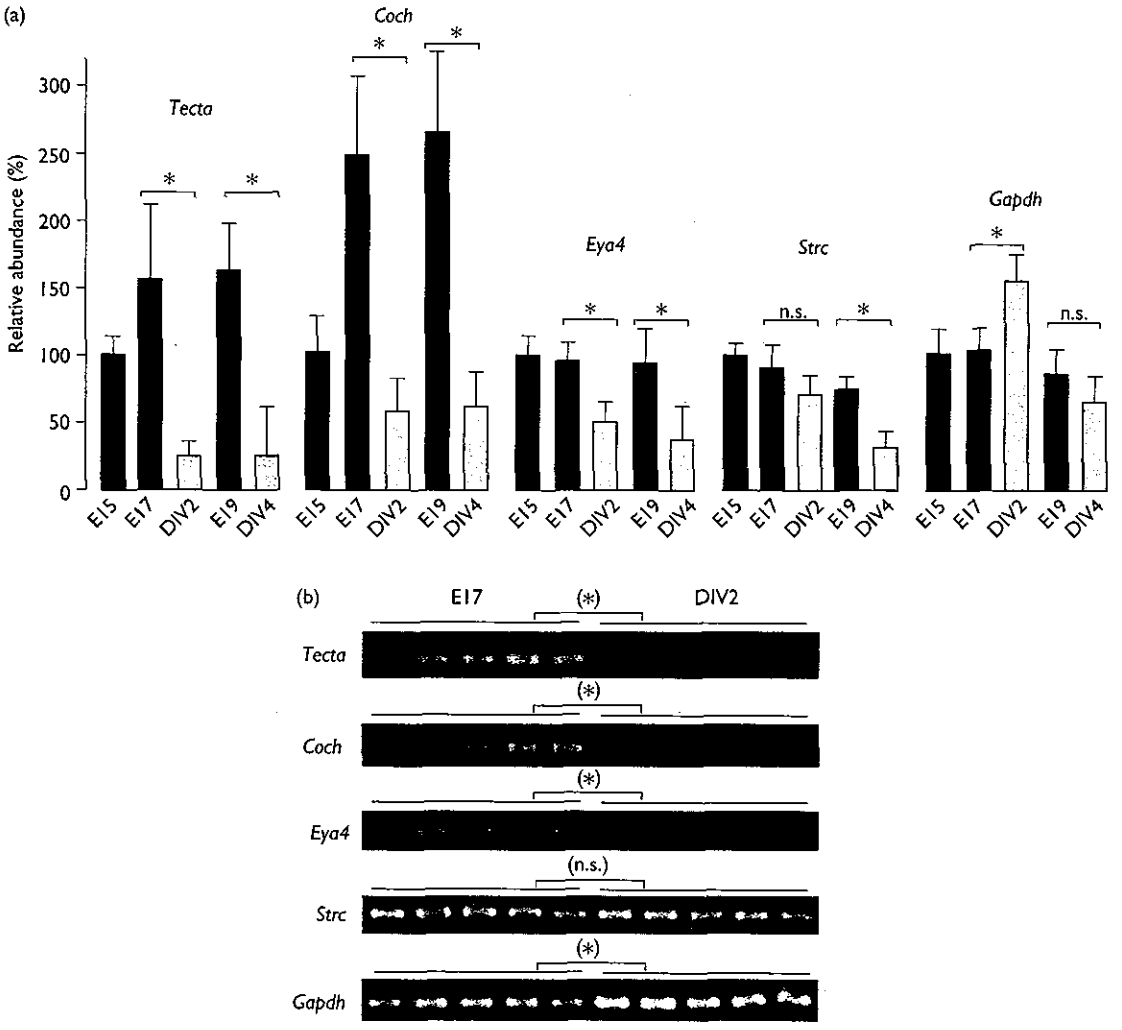

Fig. 1. (a) Relative abundance (RA) of *Tecta*, *Coch*, *Eya4*, *Strc* and *Gapdh* messenger RNA in cochlea on embryonic day 15 (E15), E17 and E19 (black bars) and at 2 days (DIV2, 48 h) and 4 days (DIV4, 96 h) *in vitro* following dissection on E15 (gray bars) expressed as a percentage of mean value on E15. RAs of *Tecta*, *Coch* and *Eya4* on DIV2 were significantly lower than that on E17. Mean RA of *Tecta* and *Coch* increased from E15 to E17 *in vivo* but not *in vitro*. RA of *Strc* on DIV2 was equivalent to that on E17. RA of *Gapdh* was significantly higher on DIV2 than on E17, and then returned to near-in-vivo level on DIV4 (one-way ANOVA and post-hoc Bonferroni method; $p<0.01$, $n=5$–7). Error bars represent SD. (b) Representative RT-PCR bands of *Tecta*, *Coch*, *Eya4*, *Strc* and *Gapdh* expression in cochlea on E17 and at DIV2. PCR was performed with number of thermocycles in mid-range of exponential phase. *Tecta*, *Coch* and *Eya4* expressions on DIV2 were less intense than on E17; *Strc* expressions on DIV2 and E17 were equivalent. *Gapdh* expression was more intense on DIV2.

MRA of *Eya4* did not change from E15 ($100\pm14\%$) to E17 ($95\pm15\%$) or E19 ($93\pm26\%$), but was significantly reduced on DIV2 ($51\pm14\%$) and DIV4 ($36\pm26\%$). Differences between DIV2 and E17 ($p<0.01$; Fig 1b, row 3), and DIV4 and E19 ($p<0.01$) were significant.

MRA of *Strc* showed no significant difference between E15 ($100\pm9\%$), E17 ($92\pm17\%$) and E19 ($74\pm10\%$), with mild reduction from E15 to E19. MRA of *Strc* on DIV2 ($71\pm16\%$) also showed mild reduction, not significantly different from that on E15 ($p>0.01$). No difference was observed in MRA between DIV2 and E17 ($p>0.05$; Fig. 1b, row 4). MRA on DIV4 ($31\pm13\%$) was significantly reduced compared with E15 and DIV2, and significantly lower than on E19 ($p<0.01$).

MRA of *Gapdh* was constant between E15 ($100\pm18.6\%$), E17 ($103\pm16\%$) and E19 ($85\pm13\%$). In the cultured cochlea, MRA increased significantly on DIV2 ($154\pm18\%$) ($p<0.01$) and was significantly higher than on E17 ($p<0.01$; Fig. 1b, row 5). MRA decreased from DIV2 to DIV4 ($64\pm20\%$) and was equivalent to E19 on DIV4 ($p>0.05$).

As represented in the low-power and high-power images, the cochlear capsule and sensory epithelilum, including a premature organ of Corti, are substantially preserved at DIV2 (Fig. 2c, d), in agreement with previous observations in studies with entire cochlear tissue explanted on E15. [14,15]. By DIV7, although the cochlear capsule and duct appear relatively undamaged (Fig. 2e), cells in the premature organ of Corti have begun to degenerate (Fig. 2f).

DISCUSSION

This cochlear explant protocol permits detection of the cochlear-specific genes *in vitro* at 48 h after dissection. Premature organ of Corti was preserved after 48 h at the light-microscopic level. We could easily verify expression of

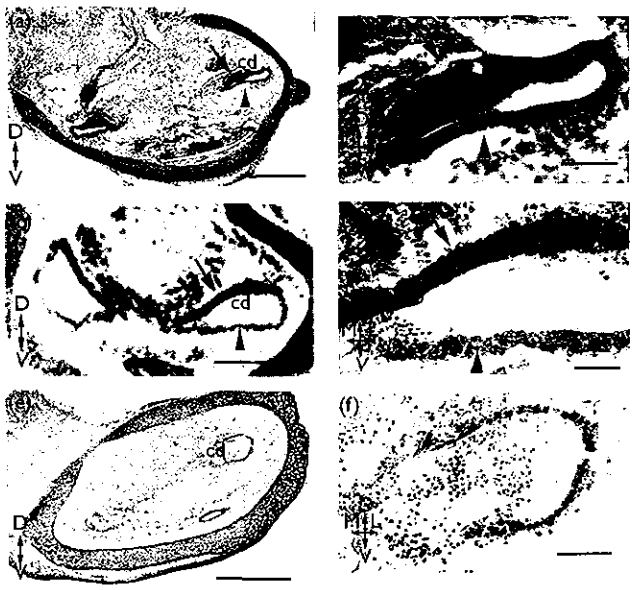

Fig. 2. Low-magnification image of cochlear tissue on embryonic day 15 (E15) (a), 2 days (DIV2, 48 h) (c) and 7 days (DIV7, 168 h) *in vitro* (e). High-power image of sensory epithelium of cochlear duct (cd) on E15 (b), DIV2 (d) and DIV7 (f). On DIV2, the premature organ of Corti comprising the dorsal wall of the immature cochlear duct (arrow), the ventral wall of the cochlea duct (arrowhead) and surrounding mesenchyme (m) are substantially preserved at the light-microscopic level. (a) and (b) represent the premature organ of Corti in the dorsal wall of the cochlear duct on E15, and one to two layers of cuboidal epithelium on the ventral wall *in vivo*. Tectorial membrane is not discernible at this stage. Dorsal (D), ventral (V), modiolar (M) and lateral (L) directions are indicated. Scale bar represents 300 μm (a, c, e) and 50 μm (b, d, f).

the cochlear-specific genes; however, we found that transcript levels were not necessarily equivalent to those found in the in-vivo condition. Specifically, *Strc* expression at DIV2 was equivalent to that *in vivo*, although *Eya4* expression was significantly lower, and *Tecta* and *Coch* expression did not demonstrate the normal surge observed between E15 and E17.

Recent techniques such as RNA interference [19] and antisense oligonucleotide inhibition [20,21] have made the controlling of expression levels of specific genes a reality. One drawback to the evaluation of these techniques for inner ear gene therapy is the lack of intrinsic expression of many of these genes in readily available cell lines. Our demonstration of expression of cochlear-specific genes in explanted tissue is significant, and makes these explants a valuable tissue source in which to investigate various techniques to regulate gene expression.

We used RT-PCR analysis to quantify expression levels of four genes and documented differential modulations in levels at DIV2. The expression of each gene, however, was reduced after an additional 48 h in culture when compared with in-vivo levels. In contrast, expression levels of *Gapdh* temporarily increased at DIV2, as compared with levels at E15 and E17. *Gapdh* encodes a glycolytic protein that catalyzes oxidative phosphorylation of glyceraldehyde-3-phosphate. Its expression is usually constant under experimental conditions both *in vivo* and *in vitro*, but increases do occur under conditions of hypoxia, heat shock and cellular proliferation, and exposure to some growth factors [22].

In this study, it is possible that *Gapdh* induction reflects relative hypoxia after isolation of the entire cochlear tissue. The microdissected organ of Corti is reported to maintain normal morphogenesis for more than 7 days in culture, suggesting that more limited dissection may lead to better maintenance of gene expression. Sobkowicz *et al.* [16] have observed that cytodifferentiation and innervation of the organ of Corti are maintained for more than 7 days when the neonatal organ of Corti is microdissected with its corresponding sector of spiral ganglion. The isolated organ of Corti has also been utilized to study the influence of dissociated mesenchymal cells [23], retinoic acid [24,25] and Notch receptor activation [20] in hair cell differentiation [6].

To address the ultimate question of how faithfully the explanted cochlea recapitulates the in-vivo cochlea at the gene-expression level, the use of microarray-based technologies would be valuable. However, PCR-based analysis offers the ability to detect precise changes in the expression of specific genes in small tissues of cochleae. Our study shows that it is feasible to quantify the expression of cochlear-specific genes in explanted tissue, especially within 48 h of explantation. Further studies are warranted, as cochlear explants will be a useful tool for assessing modulation in the expression of cochlear-specific genes under different experimental conditions.

CONCLUSION

The expressions of *Strc*, *Eya4*, *Tecta* and *Coch* were verified *in vitro* at 48 h in this explant protocol. Semiquantitative RT-PCR revealed that *Strc* expression at DIV2 was equivalent to that *in vivo*, *Eya4* expression was lower, and *Tecta* and *Coch* expression did not demonstrate the normal surge observed between E15 and E17. Although transcript levels were not necessarily equivalent to those *in vivo*, the present result demonstrates feasibility of explanted cochleae for testing modulation of expression of the cochlear-specific genes *in vitro*.

REFERENCES

1. Verhoeven K, Van Laer L, Kirschhofer K, Legan PK, Hughes DC, Schatteman I *et al.* Mutations in the human alpha-tectorin gene cause autosomal dominant non-syndromic hearing impairment. *Nat Genet* 1998; **19**:60–62.
2. Robertson NG, Lu L, Heller S, Merchant SN, Eavey RD, McKenna M *et al.* Mutations in a novel cochlear gene cause DFNA9, a human nonsyndromic deafness with vestibular dysfunction. *Nat Genet* 1998; **20**:299–303.
3. Wayne S, Robertson NG, DeClau F, Chen N, Verhoeven K, Prasad S *et al.* Mutations in the transcriptional activator *EYA4* cause late-onset deafness at the DFNA10 locus. *Hum Mol Genet* 2001; **10**:195–200.
4. Verpy E, Masmoudi S, Zwaenepoel I, Leibovici M, Hutchin TP, Del Castillo I *et al.* Mutations in a new gene encoding a protein of the hair bundle cause non-syndromic deafness at the DFNB16 locus. *Nat Genet* 2001; **29**:345–349.
5. Legan PK, Rau A, Keen JN, Richardson GP. The mouse tectorins. Modular matrix proteins of the inner ear homologous to components of the sperm–egg adhesion system. *J Biol Chem* 1997; **272**:8791–8801.
6. Rau A, Legan PK, Richardson GP. Tectorin mRNA expression is spatially and temporally restricted during mouse inner ear development. *J Comp Neurol* 1999; **405**:271–280.
7. Maeda Y, Fukushima K, Kasai N, Maeta M, Nishizaki K. Quantification of *TECTA* and *DFNA5* expression in the developing mouse cochlea. *Neuroreport* 2001; **12**:3223–3226.

8. Khetarpal U. DFNA9 is a progressive audiovestibular dysfunction with a microfibrillar deposit in the inner ear. *Laryngoscope* 2000; 110:1379–1384.
9. Robertson NG, Resendes BL, Lin JS, Lee C, Aster JC, Adams JC *et al.* Inner ear localization of mRNA and protein products of *COCH*, mutated in the sensorineural deafness and vestibular disorder, DFNA9. *Hum Mol Genet* 2001; 10:2493–2500.
10. Sher AE. The embryonic and postnatal development of the inner ear of the mouse. *Acta Otolaryngol Suppl* 1971; 285:1–77.
11. Lim DJ, Anniko M. Developmental morphology of the mouse inner ear. A scanning electron microscopic observation. *Acta Otolaryngol Suppl* 1985; 422:1–69.
12. Anniko M. Embryogenesis of the mammalian inner ear. III. Formation of the tectorial membrane of the CBA/CBA mouse *in vivo* and *in vitro*. *Anat Embryol (Berl)* 1980; 160:301–313.
13. Van De Water TR. Effects of removal of the statoacoustic ganglion complex upon the growing otocyst. *Ann Otol Rhinol Laryngol Suppl* 1976; 85:2–32.
14. Anniko M, Van de Water TR, Nordemar H. Organ culture of the 16th gestation day mouse labyrinth. A model suggestion for pre- and post-partum development. *Acta Otolaryngol* 1978; 86:52–55.
15. Tamura K, Nishizaki K, Takeda Y, Sumida S, Masuda Y. Suspension organ culture of the fetal mouse ear. *Auris Nasus Larynx* 1993; 20:239–246.
16. Sobkowicz HM, Loftus JM, Slapnick SM. Tissue culture of the organ of Corti. *Acta Otolaryngol Suppl* 1993; 502:3–36.
17. Sobkowicz HM, Rose JE. The ultrastructure of the developing organ of Corti of the mouse in culture. In: Friedmen BJI (ed.). *Ultrastructural Atlas of the Inner Ear*. London: Butterworths; 1984. pp. 61–97.
18. Utsugisawa K, Tohgi H, Yoshimura M, Nagane Y, Ukitsu M. Quantitation of nicotinic acetylcholine receptor subunits alpha 4 and beta 2 messenger RNA in postmortem human brain using a non-radioactive RT-PCR and CCD imaging system. *Brain Res Brain Res Protoc* 1999; 4:92–96.
19. Caplan NJ. Gene therapy progress and prospects. Downregulating gene expression: the impact of RNA interference. *Gene Therapy* 2004; 11:1241–1248.
20. Zine A, Van De Water TR, de Ribaupierre F. Notch signaling regulates the pattern of auditory hair cell differentiation in mammals. *Development* 2000; 127:3373–3383.
21. Delprat B, Boulanger A, Wang J, Beaudoin V, Guitton MJ, Venteo S *et al.* Downregulation of otospiralin, a novel inner ear protein, causes hair cell degeneration and deafness. *J Neurosci* 2002; 22:1718–1725.
22. Suzuki T, Higgins PJ, Crawford DR. Control selection for RNA quantitation. *Biotechniques* 2000; 29:332–337.
23. Montcouquiol M, Kelly MW. Planar and vertical signals control cellular differentiation and patterning in the mammalian cochlea. *J Neurosci* 2003; 23:9469–9478.
24. Kelley MW, Xu XM, Wagner MA, Warchol ME, Corwin JT. The developing organ of Corti contains retinoic acid and forms supernumerary hair cells in response to exogenous retinoic acid in culture. *Development* 1993; 119:1041–1053.
25. Lefebvre PP, Malgrange B, Staecker H, Moonen G, Van de Water TR. Retinoic acid stimulates regeneration of mammalian auditory hair cells. *Science* 1993; 260:692–695.

Acknowledgements: This work was partly supported by a grant from Ministry of Health, Welfare and Labor and Ministry of Science, Sports and Education of Japan and ROI-DC02842 (R.J.H.S.). There is no conflict of interest on this manuscript, including financial, consultant, institutional and other.

Renew Your Subscription Online!

Visit our Subscription Renewal Center at

LWW.com/journals/renew

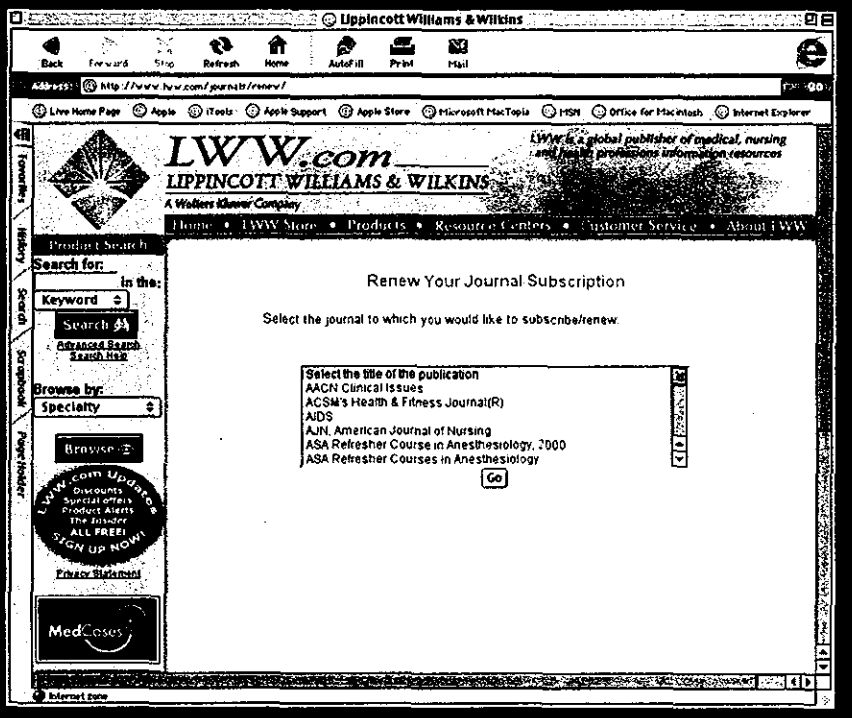

SAVE TIME...

with the ease and speed of online subscription renewal

SAVE MONEY...

by subscribing for up to 3 years at the current rates!

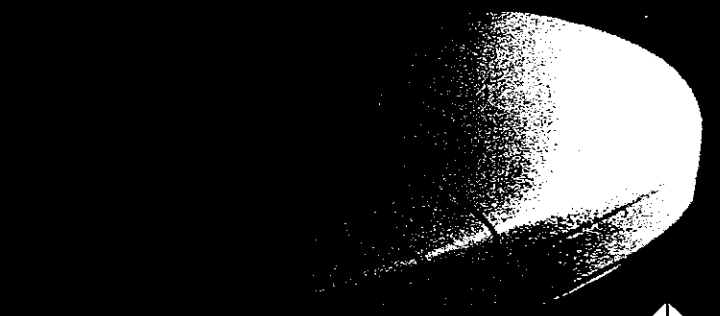

LIPPINCOTT WILLIAMS & WILKINS

A2P833F

REPRINTED FROM *ANNALS OF OTOLOGY, RHINOLOGY & LARYNGOLOGY*
May 2004 Volume 113 Number 5

CLINICAL FEATURES OF BILATERAL PROGRESSIVE HEARING LOSS ASSOCIATED WITH MYELOPEROXIDASE–ANTINEUTROPHIL CYTOPLASMIC ANTIBODY

DAI TAKAGI, MD
YUJI NAKAMARU, MD
SHIROH MAGUCHI, MD
YASUSHI FURUTA, MD
SATOSHI FUKUDA, MD
SAPPORO, JAPAN

In this study, we analyzed the clinical features, diagnostic criteria, treatment, and outcome of atypical bilateral progressive hearing loss associated with myeloperoxidase–antineutrophil cytoplasmic antibody (MPO-ANCA). The evaluation was made by audiogram and laboratory data in 6 cases treated at Hokkaido University Hospital. We measured MPO-ANCA by enzyme-linked immunosorbent assay; the result was positive in all cases. The hearing loss developed bilaterally and progressed to total deafness within several weeks. The onset of hearing loss was not simultaneous in the 2 ears. Methylprednisolone pulse therapy was effective in 9 ears. Three ears showed no improvement; 2 of the 3 ears had already exhibited total deafness at the first visit. After the treatment, the titer of MPO-ANCA decreased in all patients. The level of MPO-ANCA should be tested in patients with bilateral progressive hearing loss of unknown origin and can be used as a marker of the disease's activity.

KEY WORDS — hearing loss, immunosuppressive agent, microscopic polyangiitis, myeloperoxidase–antineutrophil cytoplasmic antibody, prednisolone.

INTRODUCTION

It has been suggested that there appears to be a form of bilateral hearing loss that is distinct from other forms of hearing loss in its clinical features, laboratory test results, and response to immunosuppressive treatment.[1] The term autoimmune inner ear disease was first proposed by McCabe[2] to describe this entity. Although several investigations of autoantibodies against inner ear antigenic epitopes or cross-reacting antibodies have been performed,[3] the pathogenesis and a diagnostic clinical marker of the disease still remain undetermined.

Antineutrophil cytoplasmic antibody (ANCA) is an autoantibody against either proteinase 3[4] or myeloperoxidase (MPO)[5] that is expressed in the neutrophil granules.[4] It is known that proteinase 3–ANCA is highly specific for Wegener's granulomatosis (WG) and that MPO-ANCA is positive in Churg-Strauss syndrome and microscopic polyangiitis (MPA). Therefore, these diseases have been referred to as certain types of ANCA-associated small-vessel vasculitis.[6] Although there have been several reports of otologic manifestations in WG or Churg-Strauss syndrome,[7,8] MPA involving the ear has been rare.

In addition, no study has analyzed the association between autoimmune hearing loss and a positive titer of MPO-ANCA. In this report, we present 6 cases of MPO-ANCA–positive hearing loss and analyze the clinical course, the outcome of treatment, and the prognosis of hearing loss to elucidate the above-mentioned association.

SUBJECTS AND METHODS

Subjects. Eight patients who showed progressive hearing loss of unknown origin and had a positive test result for MPO-ANCA were treated at Hokkaido University Hospital between 1997 and 2002. One patient had a histologic diagnosis of WG and another of relapsing polychondritis; both were excluded from the study. The remaining 6 patients, 1 man and 5 women, participated in this study. Maguchi et al[9] previously reported case 1 as a case report. The patients' ages at the time of onset ranged from 36 to 82 years.

Measurement of MPO-ANCA. We measured MPO-ANCA with an enzyme-linked immunosorbent assay. For determination of MPO-ANCA, a titration kit (MPO-ANC II, Nipro, Osaka, Japan) was used according to the manufacturer's protocol. Briefly, sera were diluted 500 times by the dilution liquid. Then, 50 μL of this material or standard solution (1,280, 640, 160, 40, and 10 U) was added to a streptavidin-bound microplate with biotin-labeled MPO antigen and incubated for 1 hour at room temperature. The wells were washed 3 times, and 200 μL of alkaline phosphatase–labeled anti-human IgG was added to

From the Department of Otolaryngology–Head and Neck Surgery, Hokkaido University Graduate School of Medicine, Sapporo, Japan.
CORRESPONDENCE — Dai Takagi, North 15 West 7, Kita-ku, Dept of Otolaryngology–Head and Neck Surgery, Hokkaido University Graduate School of Medicine, Sapporo, 060 8638 Japan.

TABLE 1. CLINICAL FINDINGS AND OTHER ORGAN INVOLVEMENT

Case No.	Age (y)	Sex	Ear Findings	Facial Palsy	CT Findings of Mastoid Cavities	Other Organ Involvement	MPO-ANCA Level (U)	Former Treatment
1	36	F	Normal*	No	Normal		74	Low-dose steroids
2	59	F	OME	No	Cloudy	Lung	13	Low-dose steroids
3	45	F	OME	Yes	Cloudy		268	Low-dose steroids and tube insertion
4	82	M	OME	No	Cloudy		15	Tube insertion
5	66	F	OME	No	Cloudy	Lung and kidney	443	Tube insertion
6	54	F	OME	No	Cloudy	Nose and eye	23	

CT — computed tomographic, MPO-ANCA — myeloperoxidase–antineutrophil cytoplasmic antibody, OME — otitis media with effusion.
*Patient developed vertigo.

each well and incubated for 1 hour at room temperature. The wells were then washed 3 times, and 100 μL of *p*-nitrophenylphosphate was added. These wells were incubated for 30 minutes at room temperature, and the absorbance at 405 nm was measured. Samples with a titer of more than 10 U were considered to have a positive result. We also examined ANCA by indirect immunofluorescence (IIF) assay according to the method used by van der Woude et al.[10]

Audiometric Evaluation. Two factors were used to evaluate the outcome of hearing loss associated with MPO-ANCA: the severity of hearing loss and the time between the onset of hearing loss and the initiation of therapy. The pure tone average was indicated as the mean of 5 frequencies: 250, 500, 1,000, 2,000, and 4,000 Hz. Hearing recovery was classified in 1 of 3 categories: complete recovery (final pure tone average of 30 dB or less), moderate recovery (improvement of more than 30 dB), and no change (improvement of less than 30 dB).

RESULTS

Table 1 presents the otologic features and the extent to which other organs were involved with hearing loss associated with MPO-ANCA. The hearing loss was bilateral in all patients and progressed over several weeks. There were 6 ears with mixed hearing loss and 6 with sensorineural hearing loss. The hearing in 3 ears had already deteriorated to complete deafness by the first visit to our clinic. In 3 patients (cases 3, 4, and 6), auditory brain stem responses and speech audiograms were obtained. The auditory brain stem responses showed normal peak and interpeak latencies. The maximum articulation scores on the speech audiograms ranged from 20% to 85%. These audiological findings suggested that the patients' hearing loss could be attributed to inner ear lesions. Vertigo developed in 3 patients (cases 1, 3, and 6), and facial nerve palsy developed in 1 patient (case 3) after the onset of hearing loss. Effusion in the middle ear was present in 5 patients, but there were no granulomatous lesions. In 1 patient (case 1), the tympanic membrane was found to be normal. A computed tomographic scan of the temporal bone revealed opacification of the mastoid cavities in all cases except case 1, but there was absolutely no evidence of invasive bony disease. Middle ear effusion was cultured for tuberculosis and other bacteria, and all results were negative. The titers of MPO-ANCA at the first examination ranged from 13 to 443 U, and an IIF assay revealed perinuclear patterns (p-ANCA) in all of the patients.

Further examinations for autoantibodies produced normal results except for antinuclear antibodies in cases 4 and 6 and rheumatoid factor in case 3. Examinations of all patients yielded negative results on *Treponema pallidum* hemagglutination assay, as well as normal eosinophil levels. Before referral to our hospital, 3 of the patients had been treated with tympanostomy tube placement and 3 with low-dose pred-

TABLE 2. TREATMENT AND OUTCOME

Case No.	Treatment			Audiological Manifestation (dB)		Outcome		Posttreatment MPO-ANCA Level
	Methylprednisolone Pulse Therapy	Cyclophosphamide	Azathioprine	Right	Left	Right	Left	
1	+			45	79	CR	No change	12 U
2	+	+		Deaf	96	MR	MR	Negative
3	+		+	Deaf	86	No change	CR	Negative
4	+			82	82	CR	MR	Negative
5	+			90	70	MR	MR	17 U
6	+			Deaf	43	No change	CR	Negative

CR — complete recovery, MR — moderate recovery.

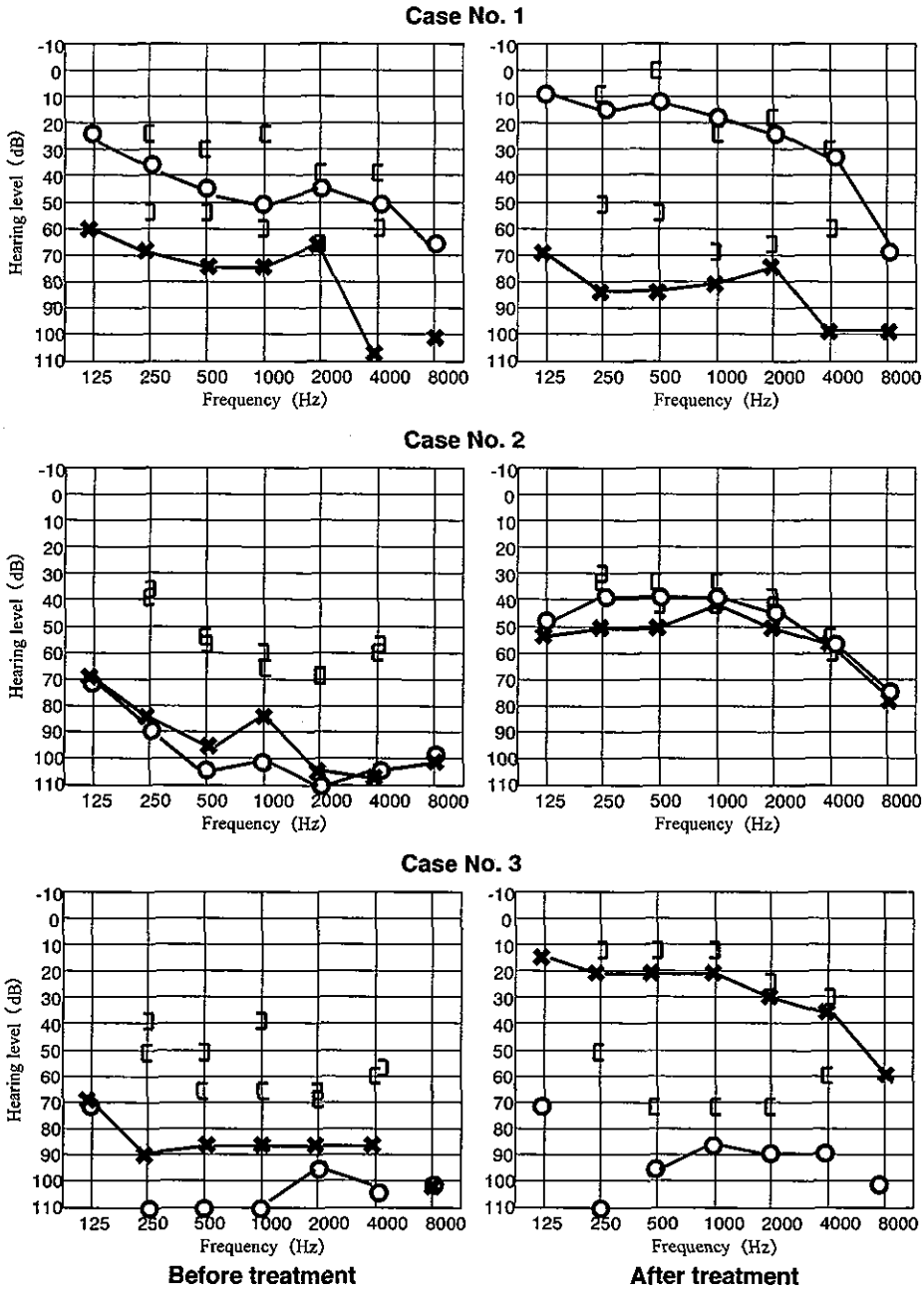

Fig 1. Pretreatment and posttreatment audiograms of cases 1, 2, and 3. After treatment, hearing level improved to normal range in right ear of case 1 and left ear of case 3.

nisolone. The hearing level of the affected side did not recover in 2 of the 3 patients treated with prednisolone and only slightly recovered in the remaining patient. In addition, when use of the drug was tapered off, the hearing level on the opposite side became worse.

In 1 patient (case 5), proteinuria and hematuria were detected after the onset of hearing loss. This female patient received a diagnosis of MPA after a transcutaneous renal biopsy.

We further analyzed the protocol of treatment and outcomes (Table 2). All 6 patients were treated with methylprednisolone pulse therapy (1 g/d) for 3 days followed by oral prednisolone. In 2 patients (cases 4 and 5), we used a half-dose of methylprednisolone (500 mg/d), because one was elderly and the other had diabetes mellitus. Two patients received oral immunosuppressive agents (cyclophosphamide or azathioprine, 100 mg/d) in addition to steroids. Four ears achieved complete recovery of hearing. Five ears recovered moderately, but in 3 of the ears the hearing level did not change after methylprednisolone pulse therapy. Of the 3 ears that exhibited complete deafness at the initial visit, 1 achieved moderate improvement, but 2 showed no improvement. Pretreatment and posttreatment audiograms of the 6 cases are shown in Figs 1 and 2. In addition, in case 5 the re-

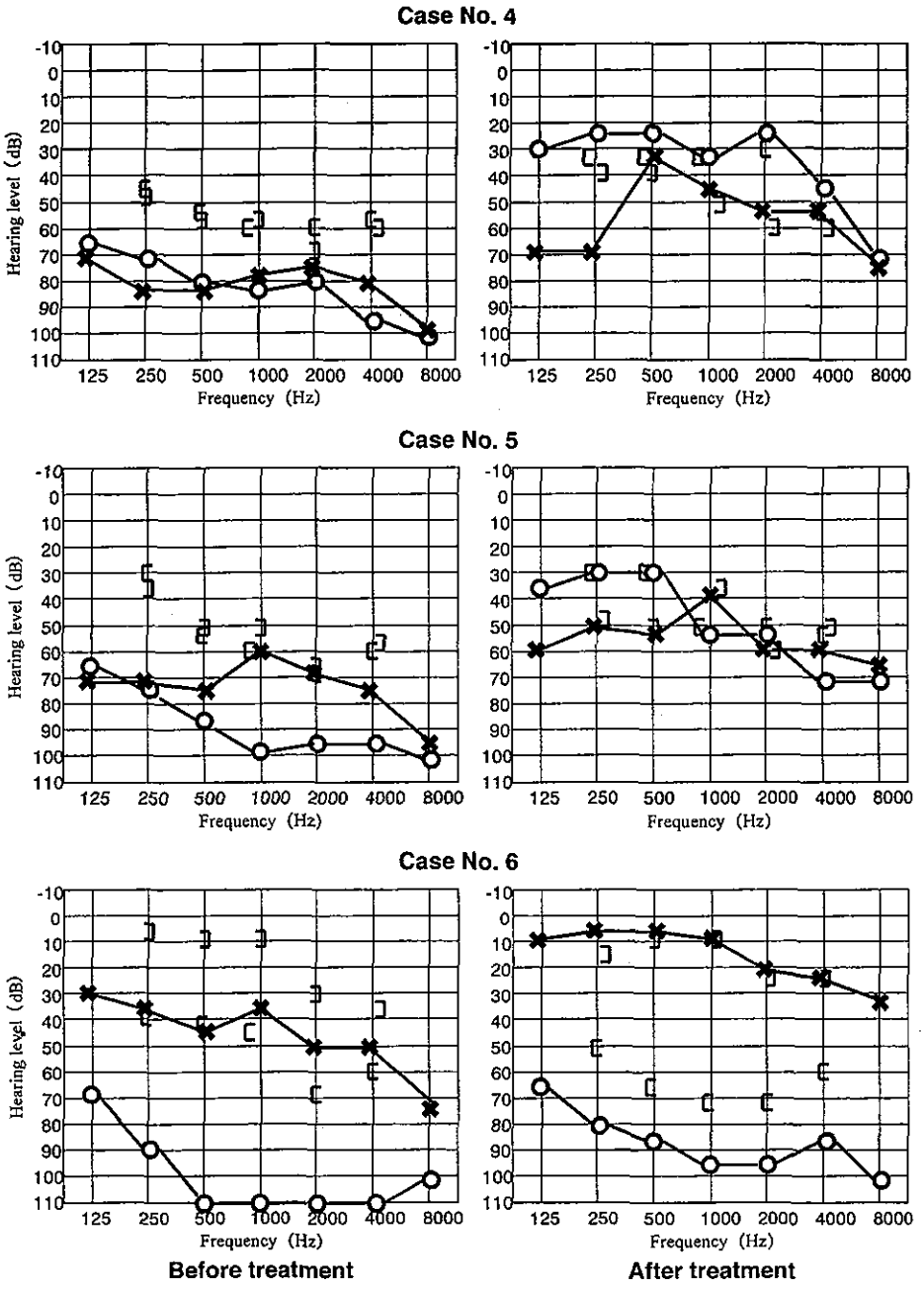

Fig 2. Pretreatment and posttreatment audiograms of cases 4, 5, and 6. After treatment, hearing level improved to normal range in right ear of case 4 and left ear of case 6.

nal function recovered after pulse therapy. The titer of serum MPO-ANCA decreased after treatment in all patients (Table 2). Drug-induced leukopenia with severe infection and cystitis were not observed in any of the 6 patients.

Furthermore, we investigated all 12 ears looking at the association between treatment outcome and the duration of hearing loss. In all 6 cases, unilateral hearing loss occurred initially, and subsequently the opposite side was affected and the condition exacerbated. The time from the onset of hearing loss to the initiation of pulse therapy ranged from 6 to 18 weeks. Four of the 5 ears in which treatment was started within 2 months of the onset of hearing loss achieved complete recovery. By contrast, none of the 7 ears in which treatment was started 2 months or more after the onset of hearing loss recovered completely (Table 3).

DISCUSSION

The results of the present study clearly indicate the necessity of measuring MPO-ANCA in patients with progressive hearing loss of unknown origin. After McCabe[1,2] proposed the clinical entity of autoimmune sensorineural hearing loss, an attempt to identify inner ear autoantigens or autoantibodies was made.[3] However, the autoantibodies directed against inner ear antigenic epitopes or cross-reacting antibodies

TABLE 3. INITIATION OF TREATMENT AND OUTCOME

*Initiation of Treatment**	*No. of Ears*	*Outcome*		
		CR	*MR*	*No Change*
Within 2 mo	5	4	1	0
2 to 4 mo	4	0	3	1
More than 4 mo	3	0	1	2

*Duration between onset of hearing loss and initiation of treatment.

remain unknown. Therefore, although the diagnosis of autoimmune sensorineural hearing loss has been made clinically,[2] no marker has been found that adequately reflects the disease's activity. In the present study, there were 6 cases of bilateral progressive hearing loss that were positive for MPO-ANCA.

MPO-ANCA, which was identified by Falk and Jennette,[11] has been used as a clinical serologic marker for the diagnosis of vasculitis-associated crescentic glomerulonephritis.[12] In our series, all patients had positive results for MPO-ANCA after the first test, and titers of MPO-ANCA were decreased as the disease began to improve after pulse therapy. These results suggest that MPO-ANCA may be a useful clinical marker not only for the diagnosis, but also for monitoring the disease's activity in patients with progressive hearing loss of unknown origin.

In ANCA-associated vasculitis, small vessels such as venules, capillaries, and arterioles are preferred for histologic analysis. However, it is still not known how the autoimmune process affects the inner ear. Yoon et al[13] described findings in temporal bones of patients with polyarteritis nodosa, including severe fibrosis and new bone formation throughout the inner ear and obstructed auditory vessels. Therefore, we assume that the impairment of inner ear blood flow may have induced sensorineural hearing loss in the patients in our series.

In case 5, hearing loss developed as the initial sign of MPA, which is characterized by necrotizing small-vessel vasculitis without evidence of granulomatous lesions.[5,14] More than 80% of patients with MPA have ANCA, most often MPO-ANCA.[6] In addition, MPA is the most common cause of pulmonary-renal syndrome and is accompanied by a variety of other organ involvements. However, no report to date has described the otologic manifestations of MPA. These results suggest that even if the disease is restricted to the ear, a general investigation should be considered in patients with a positive titer of MPO-ANCA, because pulmonary and renal manifestations can be life-threatening complications.

It is difficult to make a definite histologic diagnosis of disease associated with MPO-ANCA when the disease is restricted to the ear. In WG, biopsy specimens taken from the middle ear are usually too small to render a correct diagnosis.[7] McCabe[1] also described a patient with autoimmune inner ear disease whose hearing level decreased after myringotomy. There have also been patients with WG who exhibited facial nerve paralysis after myringotomy or mastoidectomy.[15] Therefore, surgical procedures in the middle ear should be avoided in patients with autoimmune inner ear diseases.

We recommend the measurement of MPO-ANCA in cases of progressive hearing loss of unknown origin. Although the titer of MPO-ANCA was positive in our 3 cases, even after administration of low-dose steroids there is still a possibility that the titer of MPO-ANCA will become negative after the first test if the patient has been treated with steroids previously. Therefore, the measurement of MPO-ANCA should be done before the initiation of steroid therapy. Tervaert et al[16] reported that the specificity of MPO-ANCA was 99%, and in our institution no patient showed a false-positive result of MPO-ANCA. Russell et al[17] recommend confirming MPO-ANCA–positive sera with an IIF assay to maintain maximal diagnostic accuracy. Therefore, in our institution both enzyme-linked immunosorbent assay and IIF assay are used for screening of ANCA.

In this study, treatment with methylprednisolone pulse therapy and/or immunosuppressive agents was shown to be effective for hearing loss associated with MPO-ANCA. McCabe[2] recommended that autoimmune inner ear disease be treated with combined prednisolone and cyclophosphamide therapy, because it was difficult to achieve improvement with prednisolone alone. We previously reported a relapse in a patient with WG whose ear had been treated with steroid administration.[18] In MPA, Hogan et al[19] reported that the risk of death and the possibility of relapse were lower in cyclophosphamide-treated patients than in those treated with steroids alone. However, there can be severe complications involving cyclophosphamide, including cystitis, myelodysplasia, infections, and infertility, and these complications can sometimes lead to death.[20] In the present study, 3 patients failed to respond to treatment with low-dose steroids, and so the hearing loss worsened when use of the drug was tapered off. In contrast, methylprednisolone pulse therapy achieved moderate to complete improvement in some patients. Therefore, we consider that methylprednisolone pulse therapy is useful as the initial treatment, and in fact, combined immunosuppressive therapy may not always be necessary. However, if a relapse occurs during the tapering of steroids, immunosuppressive therapy should be started without delay. As for the side effects, severe drug-induced complications were not observed in our series.

There are a few reports of cases of hearing loss in patients with a positive result for MPO-ANCA; however, the clinical features of this disease are still unclear.[9] The clinical features of our cases are summarized as follows: bilateral hearing loss progressing over several weeks; no evidence of infection; occasional accompaniment by facial nerve paralysis or vertigo; effusion of middle ear often present without granulomatous lesions and destruction of temporal bone; and otologic manifestations that responded to steroid pulse therapy or immunosuppressive agents but did not respond to low-dose steroids. Hearing loss developed bilaterally and continued to worsen from several weeks to several months. The otologic symptoms occurred without pain, and the patients did not recover or worsen with low-dose steroid treatment alone. An improvement of hearing was only achieved with high-dose steroids or methylprednisolone pulse therapy.

Despite the pulse therapy, recovery of hearing loss was unsatisfactory once the ears became completely deaf. Therefore, the early initiation of the appropriate treatment was important to help prevent irreversible damage in the inner ear. Because histologic diagnosis is difficult in cases of small-vessel vasculitis localized to the ear, we recommend starting treatment on the assumption of ANCA-associated vasculitis when a positive titer of MPO-ANCA is detected in patients who fail to respond to conventional treatment such as antibiotics or low-dose steroids, and in particular when the patient exhibits the clinical features described above. In our cases, further general investigation and careful follow-up are performed, because sometimes hearing loss may be the initial sign of MPA or other lethal vasculitic disease. Otolaryngologists should be aware of the possibility of ANCA-associated vasculitis, because it is one of the few forms of atypical progressive hearing loss.

CONCLUSIONS

We reviewed 6 cases of hearing loss associated with MPO-ANCA. The hearing loss was bilateral and progressed over several weeks. Methylprednisolone pulse therapy was effective in these cases, and the titer of MPO-ANCA decreased according to disease activity; these findings suggest that MPO-ANCA can be useful in making an early diagnosis and can be used as a marker of disease activity. Once the hearing loss has progressed to total deafness, it is difficult to induce remission. Therefore, early diagnosis and appropriate initiation of therapy is important for a good hearing prognosis. Finally, otolaryngologists should include ANCA-associated vasculitis in the differential diagnosis of cases of atypical progressive hearing loss.

REFERENCES

1. McCabe BF. Autoimmune sensorineural hearing loss. Ann Otol Rhinol Laryngol 1979;88:585-9.
2. McCabe BF. Autoimmune inner ear disease: therapy. Am J Otol 1989;10:196-7.
3. Harris JP, Sharp PA. Inner ear autoantibodies in patients with rapidly progressive sensorineural hearing loss. Laryngoscope 1990;100:516-24.
4. Jenne DE, Tschopp JT, Ludemann J, Utecht B, Gross WL. Wegener's autoantigen decoded. Nature 1990;346:520.
5. Jennette JC, Falk RJ, Andrassy K, et al. Nomenclature of systemic vasculitides. Proposal of an international consensus conference. Arthritis Rheum 1994;37:187-92.
6. Jennette JC, Falk RJ. Small-vessel vasculitis. N Engl J Med 1997;337:1512-23.
7. Kempf HG. Ear involvement in Wegener's granulomatosis. Clin Otolaryngol 1989;14:451-6.
8. Ishiyama A, Canalis RF. Otological manifestations of Churg-Strauss syndrome. Laryngoscope 2001;111:1619-24.
9. Maguchi S, Fukuda S, Chida E, Terayama Y. Myeloperoxidase–antineutrophil cytoplasmic antibody–associated sensorineural hearing loss. Auris Nasus Larynx 2001;28:S103-S106.
10. van der Woude FJ, Rasmussen N, Lobatto S, et al. Autoantibodies against neutrophils and monocytes: tool for diagnosis and marker of disease activity in Wegener's granulomatosis. Lancet 1985;1:425-9.
11. Falk RJ, Jennette JC. Anti-neutrophil cytoplasmic autoantibodies with specificity for myeloperoxidase in patients with systemic vasculitis and idiopathic necrotizing and crescentic glomerulonephritis. N Engl J Med 1988;318:1651-7.
12. Arimura Y, Minoshima S, Kamiya Y, et al. Serum myeloperoxidase and serum cytokines in anti–myeloperoxidase antibody–associated glomerulonephritis. Clin Nephrol 1993;40:256-64.
13. Yoon TH, Paparella MM, Schachern PA. Systemic vasculitis: a temporal bone histopathologic study. Laryngoscope 1989; 99:600-9.
14. Nachman PH, Hogan SL, Jennette JC, Falk RJ. Treatment response and relapse in antineutrophil cytoplasmic autoantibody–associated microscopic polyangiitis and glomerulonephritis. J Am Soc Nephrol 1996;7:33-9.
15. Nicklasson B, Stangeland N. Wegener's granulomatosis presenting as otitis media. J Laryngol Otol 1982;96:277-80.
16. Tervaert JW, Goldschmeding R, Elema JD, et al. Association of autoantibodies to myeloperoxidase with different forms of vasculitis. Arthritis Rheum 1990;33:1264-72.
17. Russell KA, Wiegert E, Schroeder DR, Homburger HA, Specks U. Detection of anti-neutrophil cytoplasmic antibodies under actual clinical testing conditions. Clin Immunol 2002; 103:196-203.
18. Takagi D, Nakamaru Y, Maguchi S, Furuta Y, Fukuda S. Otologic manifestations of Wegener's granulomatosis. Laryngoscope 2002;112:1684-90.
19. Hogan SL, Nachman PH, Wilkman AS, Jennette JC, Falk RJ. Prognostic markers in patients with antineutrophil cytoplasmic autoantibody–associated microscopic polyangiitis and glomerulonephritis. J Am Soc Nephrol 1996;7:23-32.
20. Hoffman GS, Kerr GS, Leavitt RY, et al. Wegener granulomatosis: an analysis of 158 patients. Ann Intern Med 1992; 116:488-98.

REPRINTED FROM *ANNALS OF OTOLOGY, RHINOLOGY & LARYNGOLOGY*
March 2004 Volume 113 Number 3

COMPARISON OF ACUTE LOW-TONE SENSORINEURAL HEARING LOSS VERSUS MENIERE'S DISEASE BY ELECTROCOCHLEOGRAPHY

YOSHIHIRO NOGUCHI, MD
HIROAKI NISHIDA, MD
HISASHI TOKANO, MD
YOSHIYUKI KAWASHIMA, MD
KEN KITAMURA, MD
TOKYO, JAPAN

To clarify the pathogenesis of acute low-tone sensorineural hearing loss (ALHL), we retrospectively compared the electrocochleographic findings from 20 patients with ALHL with those from 58 patients with Meniere's disease (MD) classified into 4 groups (MD1 through MD4) according to their pure tone average. The mean summating potential–action potential ratio in the ALHL group was 0.35 ± 0.13, which was significantly higher than the control ratio but similar to the ratio seen in the MD1 group (pure tone average < 25 dB hearing level). The mean detection threshold of the cochlear microphonics in the ALHL group was 32.0 ± 9.4 dB normal hearing level, which was again similar to that seen in the MD1 group. Moreover, more than 50% of patients with ALHL had normal cochlear microphonics input-output curves. We therefore conclude that the pathogenesis of ALHL arises from an endolymphatic hydrops with little or no impairment of hair cells that resembles early-stage MD.

KEY WORDS — acute low-tone sensorineural hearing loss, electrocochleography, endolymphatic hydrops, Meniere's disease.

INTRODUCTION

First described by Abe[1] in 1982, acute low-tone sensorineural hearing loss (ALHL) is an independent disorder defined as a sensorineural hearing loss at lower frequencies with an acute onset and unknown cause without vertigo. The clinical features include a predominance of female sufferers; a peak incidence during the fourth decade of life; a high incidence of tinnitus, ear fullness, and/or autophony; and suspicion of bilateral involvement.[2] The prognosis shows complete or partial recovery in more than 80% of patients within 3 months.[3,4] Over the long term (>3 years), however, 27% of patients show recurrence of low-tone loss or cochlear Meniere's disease, and 11% develop classic Meniere's disease (MD).[3]

Low-tone sensorineural hearing loss is considered to be a specific audiometric configuration indicative of early-stage MD and endolymphatic hydrops (ELH). For that reason, electrocochleography (ECochG) and glycerol testing have been used to investigate the pathogenesis of ALHL. For instance, Yamasoba et al[3] reported that 63% of 38 patients studied had elevated summating potential–action potential (SP/AP) ratios; and 54% of 24 patients with ALHL had elevated SPs.[5] Glycerol testing showed positive results in 74% of 35 patients tested[3] and in 36.3% of 55 affected ears.[6] Taken together, these findings suggest that ELH might be the cause of ALHL.

The receptor potential in the hair cells in the cochlea is known as the cochlear microphonics (CM). The presence of MD or ELH is often determined with SP and AP amplitudes measured by ECochG. Measurement of the CM can provide additional detailed information about cochlear function in various inner ear diseases,[7,8] as well as a diagnosis of retrocochlear dysfunction.[9-11] In the present study, we compared ECochG findings, including CM measurements, in patients with ALHL and MD with the aim of better understanding the pathophysiology of ALHL.

PATIENTS AND METHODS

The study sample consisted of 20 patients with ALHL (8 women and 12 men; age, 21 to 61 years; mean age ± SD, 41.6 ± 11.1 years) referred to the Department of Otolaryngology, Tokyo Medical and Dental University Hospital. A diagnosis of ALHL was made at the first visit to our department according to the following criteria established by the Study Group of Sudden-Onset Hearing Loss, Japanese Ministry of Health, Labour and Welfare: 1) acute low-tone sensorineural hearing loss of unknown cause; 2) a sum of the audiometric thresholds at the frequencies 125, 250, and 500 Hz of 70 dB or more; 3) a sum of the audiometric thresholds at the frequencies 2, 4, and 8 kHz of 60 dB or less; and 4) no evidence of vertigo. We also examined 58 patients with definite MD (31 women and 27 men; age, 21 to 69 years; mean age ± SD, 47.9 ± 13.4 years), who were classified into 4 groups (MD1 through MD4) according to the guidelines for MD of the Committee on Hearing and Equilibrium of the American Academy of Otolaryngol-

From the Department of Otolaryngology, Tokyo Medical and Dental University Graduate School, Tokyo, Japan.
CORRESPONDENCE — Yoshihiro Noguchi, MD, 1-5-45, Yushima, Bunkyo-ku, Tokyo 113-8519, Japan.

TABLE 1. MENIERE'S DISEASE GROUPS

Group	*Stage*	*Pure Tone Average (dB HL)*	*No. of Patients*
MD1	1	<25	15
MD2	2	26-40	11
MD3	3	41-70	27
MD4	4	>70	5

ogy–Head and Neck Surgery (AAO-HNS).[12] One modification in the present study was that pure tone averages were calculated from thresholds at the frequencies of 0.5, 1, and 2 kHz (Table 1). Pure tone audiometry was carried out just before ECochG.

The audiograms recorded from the ALHL group and the four MD groups are superimposed in Fig 1. The pure tone averages (0.5, 1, and 2 kHz) in the ALHL, MD1, MD2, MD3, and MD4 groups were 17.5 ± 5.7 (mean ± SD), 17.4 ± 6.1, 32.4 ± 3.8, 53.4 ± 8.0, and 76.7 ± 5.2 dB hearing level (HL), respectively. There was no significant difference in pure tone average between the ALHL and MD1 groups (p = .907, Mann-Whitney U test).

Tympanic ECochG was carried out with an HN-5 electrode (Unique Medical, Tokyo, Japan) that enabled low-noise recordings with the patients lying comfortably on an examining table in a soundproof room.[13] As acoustic stimuli, short tone bursts with 1-ms rise and fall times and 3-ms durations with a frequency of 1 kHz were used to evoke CM; alternating polarity clicks were used to measure SP and AP amplitudes. The stimulus intensities ranged from 90 dB normal hearing level (nHL) down to the response threshold in 10-dB steps; and the stimuli were delivered in a free field with a distance of 50 cm between the shielded loudspeaker and the ear canal entrance. These sound stimuli were presented with an SSS-3200 sound generator (Nihon Kohden, Tokyo), and an ER-1100 with software for ECochG (GE Marquet, Tokyo) was used for recording and averaging.

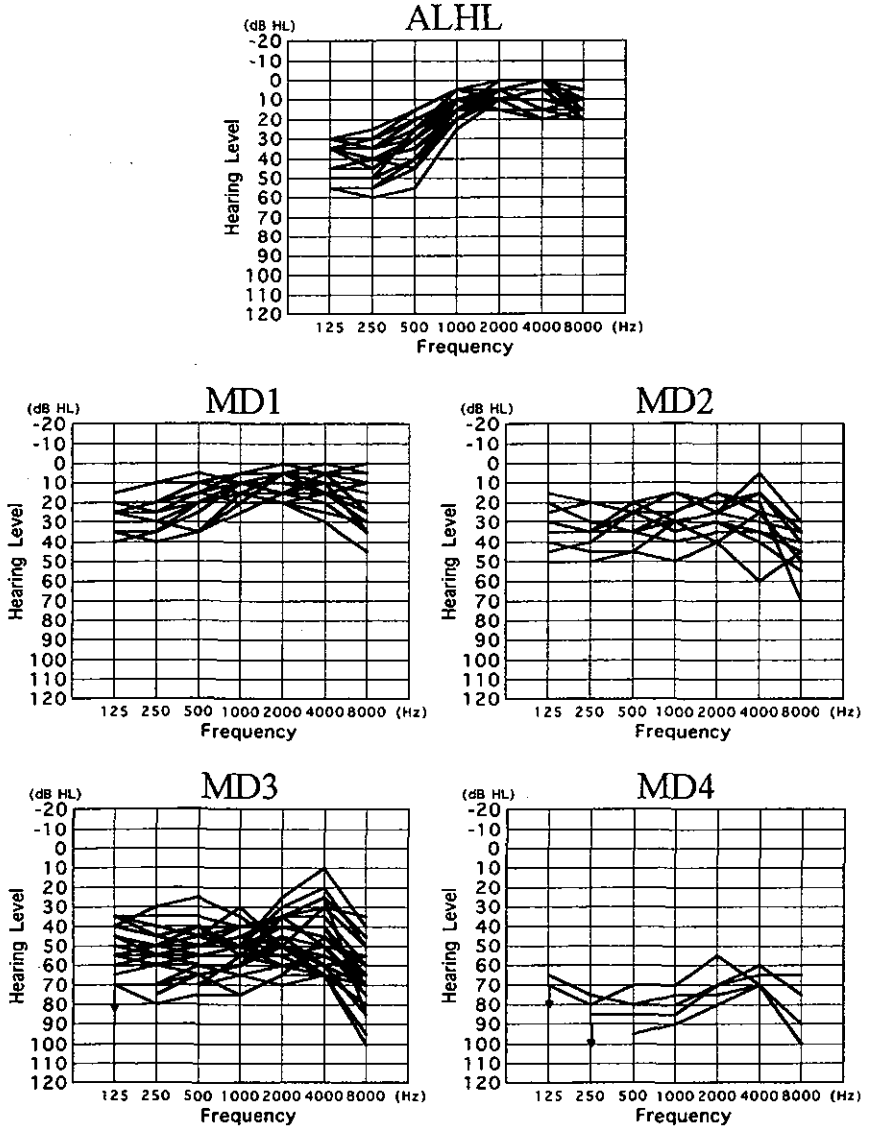

Fig 1. Overlapping audiograms recorded from patient groups with acute low-tone sensorineural hearing loss (ALHL) and Meniere's disease (MD).